









ORIGINAL PAPER

Open Access



Widespread Permian granite magmatism in Lower Austroalpine units: significance for Permian rifting in the Eastern Alps

Sihua Yuan^{1,2} , Franz Neubauer^{2*} , Yongjiang Liu^{3,4} , Johann Genser² , Boran Liu² , Shengyao Yu^{3,4} , Ruihong Chang²  and Qingbin Guan^{3,4} 

Abstract

The Grobgneis complex, located in the eastern Austroalpine unit of the Eastern Alps, exposes large volumes of pre-Alpine porphyric metagranites, sometimes associated with small gabbroic bodies. To better understand tectonic setting of the metagranites, we carried out detailed geochronological and geochemical investigations on the major part of the porphyric metagranites. LA-ICP-MS zircon U-Pb dating of three metagranites sampled from the Grobgneis complex provides the first reliable evidence for large volumes of Permian plutonism within the pre-Alpine basement of the Lower Austroalpine units. Concordant zircons from three samples yield ages at 272.2 ± 1.2 Ma, 268.6 ± 2.3 Ma and 267.6 ± 2.9 Ma interpreted to date the emplacement of the granite suite. In combination with published ages for other Permian Alpine magmatic bodies, the new U-Pb ages provide evidence of a temporally restricted period of plutonism (“Grobgneis”) in the Raabalpen basement Complex during the Middle Permian. Comparing the investigated basement with that of the West Carpathian basement, we argue that widespread Permian granite magmatism occurred in the Lower Austroalpine units. They belong to the high-K calc-alkaline to shoshonitic S-type series on the base of geochemical data. Zircon Hf isotopic compositions of the Grobgneis metagranites show $\epsilon_{\text{Hf}}(t)$ values of -4.37 to -0.6 , with T_{DM2} model ages of 1.31–1.55 Ga, indicating that their protoliths were derived by the recycling of older continental crust. We suggest that the Permian granitic and gabbroic rocks are considered as rifted-related rocks in the Lower Austroalpine units and are contemporaneous with cover sediments.

Keywords: Grobgneis, Lower Austroalpine nappes, Continental rifting, Post-Variscan granitoids, Permian event

1 Introduction

As long discussed for the Eastern and Southern Alps and testified by deposition of thick Permian sedimentary succession, Permian extension occurred in the aftermath of the Variscan orogeny (Krainer 1993 and references therein; Decarlis et al. 2013). The ongoing subsidence did leave only a short time after the Late Carboniferous (Pennsylvanian) Variscan orogeny, in the order of a few

million years, for denudation of the uplifting Variscan orogen. In the sedimentary level, thick Permian sedimentary deposits were deposited in the eastern part of the Southern Alps, which also include thick Permian acidic volcanics (Bozen quartz porphyry), Permian reefs and lagoonal evaporites deposited at the margin of the westwards transgressive Tethyan Ocean (Schaffhauser et al. 2015). In the Austroalpine units north of the Periadriatic fault, Permian deposits are generally variably thick terrestrial clastics and grading into Late Permian/Early Triassic evaporites followed by Triassic marine clastic and several km thick Middle and Upper Triassic carbonate platforms. These observations led early to the idea that Permian sedimentary deposits are rift related followed

Editorial handling: Paola Manzotti.

*Correspondence: franz.neubauer@sbg.ac.at

² Department of Geology and Geography, Paris-Lodron-University of Salzburg, 5020 Salzburg, Austria

Full list of author information is available at the end of the article



© The Author(s) 2020. This article is licensed under a Creative Commons Attribution 4.0 International License, which permits use, sharing, adaptation, distribution and reproduction in any medium or format, as long as you give appropriate credit to the original author(s) and the source, provide a link to the Creative Commons licence, and indicate if changes were made. The images or other third party material in this article are included in the article's Creative Commons licence, unless indicated otherwise in a credit line to the material. If material is not included in the article's Creative Commons licence and your intended use is not permitted by statutory regulation or exceeds the permitted use, you will need to obtain permission directly from the copyright holder. To view a copy of this licence, visit <http://creativecommons.org/licenses/by/4.0/>.

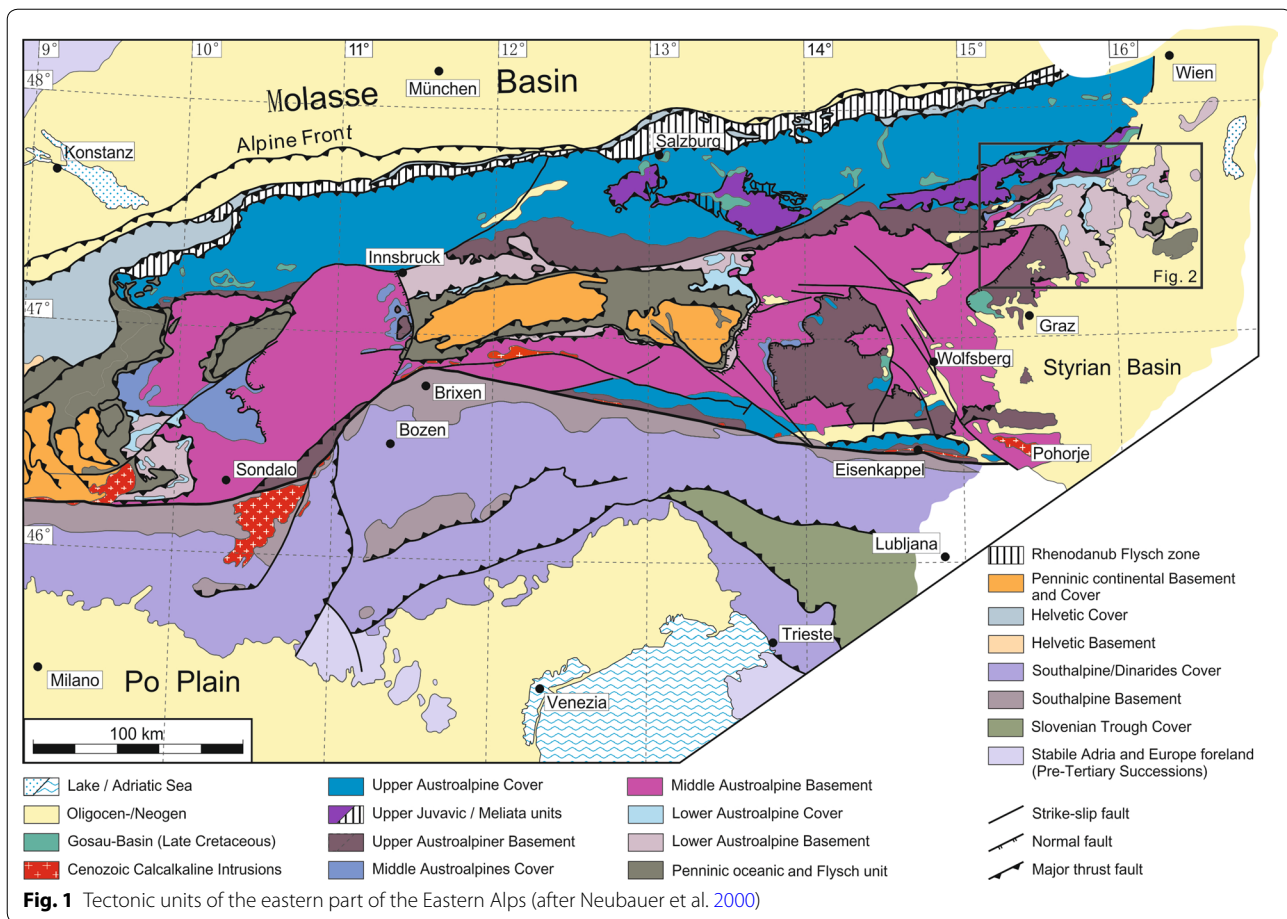
by late Ladinian opening of the Meliata oceanic rift (e.g., Kozur 1991; Neubauer et al. 2000). Ongoing geochronological work found increasing evidence for small gabbroic Permian plutonism in Austroalpine units (Thöni and Jagoutz 1992; Thöni and Miller 1996), for a small granitic orthogneiss body dated by the Rb–Sr whole rock method (Morauf 1980) and for Permian pegmatites (Schuster et al. 2001a, b; Knoll et al. 2018), but no large granite bodies. Major granitic bodies were considered Late Carboniferous, mostly based on Rb–Sr whole rock dating (Schermaier et al. 1997 and references therein), some recently confirmed by U–Pb dating (e.g., Mandl et al. 2018). On the other hand, geochronology often combined with petrological studies found increasing evidence for Permian low-pressure metamorphism (Schuster et al. 2001a, b; Schuster and Stüwe 2008; Thöni and Miller 2009; Liu et al. 2001). For the Austroalpine nappe stack in the Eastern Alps, this leaves the question open, how Permian plutonism and low-pressure metamorphism relates to sedimentary successions, whether there are some major Permian granite bodies, and which evidence argues for a coherent tectonic model. Several tectonic processes have been proposed for explanation of the Permian post-Variscan tectonic evolution of Alps and central European Variscides: (a) the onset of a rifting process that continued until the Middle Triassic crustal break-up and oceanic spreading of the Meliata Ocean (Kozur 1991; Neubauer et al. 2000, 2018; Plašienka 2018; Putiš et al. 2019); (b) post-Variscan orogenic collapse (Ménard and Molnar 1988); (c) magmatic underplating (Schuster and Stüwe 2008); (d) a back-arc extension induced by the oblique subduction of the Paleotethys ocean beneath the southern margin of the Pangea continent (Cassinis et al. 2012; Finger and Steyrer 1990; Stampfli and Kozur 2006); (e) an initial strike-slip to transtensional shearing affecting the southern side of the Variscan orogen between Eurasia and Gondwana (Muttoni et al. 2009; Schaltegger and Brack 2007), which was followed by a period of progressive extension until the Alpine rifting that began during Carnian–Norian times; (f) superplume emplacement (Doblas et al. 1998).

The “Permian event” in the European Eastern Alps (Schuster and Stüwe 2008; Thöni and Miller 2009) is a key issue to understand post-Variscan tectonic processes. In particular, Permian magmatism was reported in the Middle Austroalpine (Upper Austroalpine after Schmid et al. 2004) units, such as the Siegraben granitic orthogneiss (Putiš et al. 2002), Koralm and Saualm eclogitic complex also host Permian pegmatites (Miller et al. 2005; Thöni and Miller 1996; Knoll et al. 2018). Available Sm–Nd age data of garnet from metasediments (Wölz, Saualpe, Koralm units) are restricted to a time interval, roughly between 280 and 260 Ma (Thöni

and Miller 2009). The same age magmatism, sometimes associated with high-temperature metamorphism, is also reported from the Southern Alps (e.g. Marotta and Spalla 2007; Schaltegger and Brack 2007; Visonà et al. 2007; Peressini et al. 2007; Klötzli et al. 2014), Western Alps (Kunz et al. 2018; Manzotti et al. 2017, 2018), Western Carpathians (e.g. Pelech et al. 2017; Spišiak et al. 2018) and other parts of the southern Variscan belt (e.g. Derooin and Bonin 2003; Pereira et al. 2014; Rodríguez-Méndez et al. 2016). Despite their importance in understanding the geodynamic evolution of the Eastern Alps, until now, no reliable ages were reported from the Lower Austroalpine units such as the medium- to high-grade polymetamorphic basement rocks of the Raabalpen basement Complex, at the eastern margin of the Eastern Alps. Large volumes of porphyric metagranite, which is one of the largest remnants of seemingly “Variscan” granites in the Lower Austroalpine units (Schermaier et al. 1997) and occupies an important position at the eastern end of the Alpine chain. We present new laser-ablation ICP-MS U–Pb zircon age determinations that significantly advance our understanding of the Permian tectonomagmatic processes of the Lower Austroalpine units. By means of a combined LA-ICP-MS zircon, geochemistry and zircon Hf isotopes study of representative samples, the emplacement age of the Grobgneis granites in the Raabalpen Complex, the tectonic processes and sources involved in formation of that granitoid magmatism have been determined. We use the new data to make correlations with the adjacent areas and deduce the tectonic processes of granite formation, which give tight constraints on the link between magmatism, metamorphism and sedimentary products in a complex Permian geodynamic setting.

2 Geological setting

The Austroalpine nappe stack in the Eastern Alps represents a major portion of the Alpine edifice connected with the West Carpathians and extend over more than 1000 km throughout Austria and Slovakia. The individual nappes of the Austroalpine nappe stack contain metamorphic pre-Alpine basement covered by Permian to Mesozoic sedimentary successions, which allow a simple tectonic subdivision, for which we follow the simplified terminology after Neubauer et al. (2000), which is divided on basis of their tectonic position with respect to the ~90 Ma old eo-Alpine high-pressure wedge (Fig. 1). The Lower Austroalpine units are widespread along the eastern margins of the Eastern Alps (Fig. 1) and allow subdivision into a lower Wechsel nappe exposed mainly in the Wechsel window, and an upper Kirchberg-Stuhleck nappe (Fig. 1). In terms of basement complexes, the Lower Austroalpine unit comprises from bottom to the top the Wechsel and Waldbach Complexes within



the Wechsel window and the Raabalpen Complex with the “Grobgnais” (Fig. 2) and potentially a higher Strallegg Complex (with migmatites) (Schuster et al. 2001a; Fig. 2). A detailed description of this succession is available in Flügel and Neubauer (1984), Neubauer and Frisch (1993) and Schuster et al. (2001a) and therefore only a brief summary of the Lower Austroalpine basement units is given here.

The Wechsel Complex is mainly composed of albiteporphyroblast gneisses and structurally overlying phyllites. New LA-ICP-MS U-Pb zircon age data set gives them for two stages of magmatism at 500–520 Ma and 550–570 Ma (Neubauer et al. submitted for this issue). Müller et al. (1999) published $^{40}\text{Ar}/^{39}\text{Ar}$ ages of paragonitic mica, which yield c. 245 Ma and interpreted them as indications for a Permian–Triassic lower greenschist facies metamorphic imprint overprinting a Devonian pressure-dominated metamorphic stage.

The entirely undated Waldbach Complex consists of phyllitic micaschist at the structural base, intermediate orthogneisses (hornblende orthogneiss), various amphibolites and thin layers of garnet micaschists,

sulphide-bearing black schists and quartzites, and stratiform sulphides on the top of amphibolites (Neubauer and Frisch 1993). The stage of amphibolite facies metamorphism is believed to be the Variscan, overprinted by Late Cretaceous greenschist facies-grade metamorphism (Neubauer and Frisch 1993). Both units, the Wechsel and Waldbach Complexes, are covered by a Permian to Triassic cover with a thin unit of Permian Verrucano-type acidic volcanics, arkose and quartzphyllites at the base (Faulpl 1970).

The Raabalpen Complex is mainly composed of “Grobgnais”, a coarse-grained porphyric metagranite extending over 120 km in E–W direction and ca. 60 km in N–S direction. The host rocks of the porphyric metagranite are micaschists and quartzphyllites, with minor intercalations of talc-schists, clinopyroxene-bearing amphibolites, kyanite-bearing quartzites, paragneiss and micaschist, leucophyllites (a Mg-chlorite-quartz originally described as “white schists”) representing metasomatically altered mylonites and phyllonites after the porphyric metagranite, and tourmalinites (Flügel and Neubauer 1984; Demény et al. 1997; Neubauer et al. 1992). Metagabbros

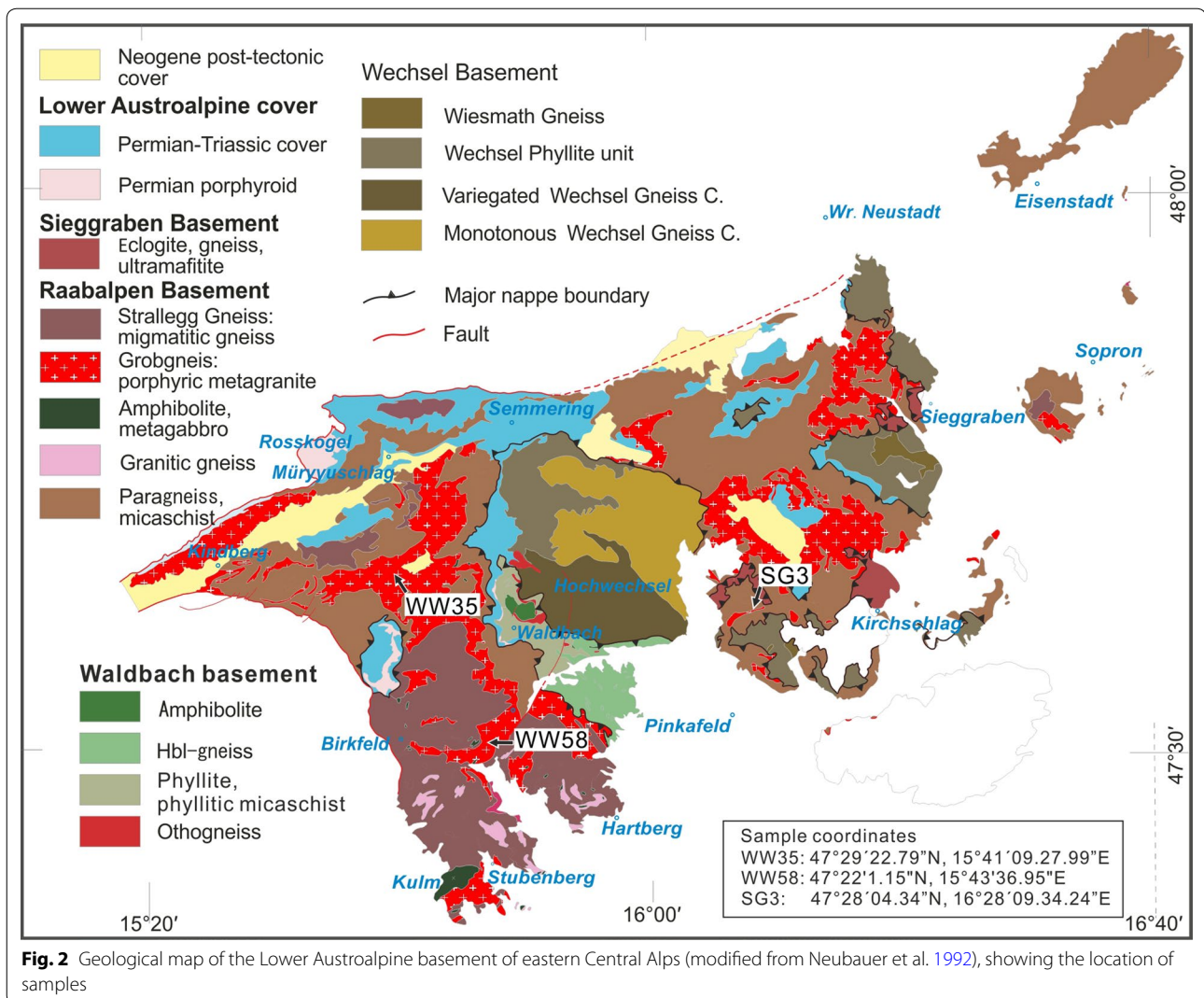


Fig. 2 Geological map of the Lower Austroalpine basement of eastern Central Alps (modified from Neubauer et al. 1992), showing the location of samples

and amphibolites occur as decameter thick lenses within paragneisses and along margins of orthogneiss bodies. The Strallegg Gneiss is a migmatitic locally aluminosilicate-bearing biotite-rich paragneiss with a stromatitic foliation.

The main metamorphic event in these units is the pre-Alpine amphibolite metamorphism within the stability field of staurolite in northern areas (basement micaschist) (Neubauer et al. 1999; Schuster et al. 2001b). The area includes in part migmatitization of the metapelites in southern areas. Lazulite-quartz veins crosscutting the micaschist are dated at 246 ± 23 Ma by the U–Th–Pb electron microprobe (EMP) method on xenotime (Bernhard et al. 1998). They argue for a hydrothermal event of Late Permian/Early Triassic age in the northernmost part of the unit. The intensity of (Early) Alpine (Late Cretaceous) metamorphism decreases from amphibolite facies conditions in the southern areas of the Raab Alps

to a greenschist facies metamorphic overprint in the northern areas, $^{40}\text{Ar}/^{39}\text{Ar}$ and Rb–Sr muscovite dating yield Cretaceous ages (70–80 Ma) for the metamorphic overprint of the upper nappe (Dallmeyer et al. 1998 and Hoinkes et al. 1999 and references therein).

Within the Raabalpen basement Complex, porphyric granitic gneisses are widespread, including the most widespread “Grobgneiss”, a small body of fine-grained, porphyric metatonalite and isolated (garnet-bearing) two-mica granite (Neubauer et al. 1992; Schermaier et al. 1997). Cross-cutting relationships combined with Rb–Sr geochronological work revealed complex intrusion relationship. The widespread “Grobgneiss” is a coarse-grained, porphyric, sheet-like granite gneiss with rare lenses of tonalite gneiss. The Rb–Sr whole-rock age of the Grobgneiss is 338 ± 12 Ma (Neubauer et al. 1992; Schermaier et al. 1997). But new geochronological investigations of (Tropper et al. 2007) on Stubenberg granites yield ages

of 263 ± 16 Ma and 265 ± 31 Ma (zirconolite Th–U–Pb dating using EMP), which are interpreted to be the age of their formation. Metagabbro and diorite with well-preserved magmatic fabric occur along the margins of the Grobgnais, e.g. the gabbros of Birkfeld and Landsee. A crystallization age of 264 ± 7 Ma was determined for a gabbro by the Sm–Nd method and zircon ages in the same range are reported for the orthogneisses from the same area (Schuster et al. 2001b). Further metagabbro occurrences are found within amphibolites of the Kulm at the southwestern margin of the Grobgnais. These metagabbros may be of Permian age because they postdate the pre-Alpine metamorphism (Schuster et al. 2001b).

The Raabalen Complex including the Grobgnais of the Lower Austroalpine units is also covered by Permian to Triassic sediments. The succession starts with conglomerates, pebbly sandstones and quartzitic schists summarized as “Alpine Verrucano”. Lower Triassic Semmering Quartzite follows. It is worth noting that the Permian to Lower Triassic clastic sediments vary in thickness between few tens to ~ 1000 m, apparently reflecting extensional “graben” tectonics. Permian extrusive rocks within the basal cover successions are acidic volcanics (e.g., “Roßkogel Porphyroid”; Nievoll, 1984; Neubauer 1988).

3 Sample description

Three samples of representative, spatially distant locations were selected for the present LA-ICP-MS zircon U–Pb and Hf isotopic study to define their ages; one from the main body of the Grobgnais in the northwestern area (WW35; $47^{\circ} 29' 22.79''$ N, $15^{\circ} 41' 27.99''$ E), one in the south (WW58; $47^{\circ} 22' 1.15'''$ N, $15^{\circ} 43' 36.95'''$ E) and one in the east (SG3, $47^{\circ} 28' 4.34''$ N, $16^{\circ} 9' 34.24''$ E). Beside the samples for dating, several further samples around the dating sample location were selected for further chemical analysis to elucidate the petrogenesis and tectonic significance of their protoliths. These further samples are similar in mineralogy and fabrics but show varying mineral proportions.

The Grobgnais is a K-feldspar porphyroclasts-bearing orthogneiss (Fig. 3a). Its characteristic feature is the presence of light pink potassium feldspar crystals (1 to 5 cm in length) (Fig. 3a) with respectable twinning, which are suspended in a groundmass of finer grains of plagioclase, K-feldspar and quartz (Fig. 3b, d). The mineral assemblage of the samples is quartz (25–30%), K-feldspar (30–35%), plagioclase (20–35%) and muscovite (10%), with minor amounts of garnet (Fig. 3b) and accessory minerals (e.g., apatite, zircon, and opaque Fe–Ti oxides). Intense shearing has locally imparted a protomylonitic fabric (Fig. 3c). Commonly, the deformational overprint is limited to specific shear zones, which show pervasive

overprint. The porphyroclasts disturbed the foliation which is characterized by aligned muscovites and quartz aggregates forming the matrix (Fig. 3c, d). The porphyroclast display remnants of pre-existing megacrysts when the size is diminished by syn-deformational recrystallization. Several signatures of brittle and ductile deformation are observed. The quartz deformation behaviours include elongation, grain boundary migration, undulose extinction and different degrees of dynamic recrystallization, formation of recrystallized new grains of the matrix commonly flank the porphyroclasts, forming mantled porphyroclast structure. Muscovite occurs often in two generations, large old flakes (muscovite I), which are often recrystallized along margins or replaced by fine-grained muscovite II during Cretaceous metamorphism (Fig. 3d). Quartz aggregates and muscovites are often deformed into wings that extend on the both sides of the K-feldspar porphyroclast. The material behaviour of quartz and feldspars indicates that deformation occurred under a temperature of about ± 500 °C (Passchier and Trouw 1998).

4 Analytical methods

4.1 LA-ICP-MS zircon U–Pb dating

All samples using standard technique of density and magnetic separation in the Laboratory of Langfang Regional Geological Survey, Hebei Province. Approximately 1 to 2 kg of each sample was crushed using a jaw crusher. The crushed material was sieved to extract the grain size between 0.072 and 0.400 mm. The Franz magnetic separator was then used to separate magnetic minerals from non-magnetic minerals. Zircons were separated by using heavy liquid and then hand-picked under a binocular microscope. All representative zircon grains of each sample were categorized based on color and morphology and then mounted in epoxy resin. Zircon mounts were polished until the cores of most grains were exposed. Before analysis, the surface was cleaned by using 3% (v/v) HNO_3 to remove any lead contamination. Cathodoluminescence (CL) images were obtained for zircons prior to analysis, using a Mono CL3+ microprobe, in order to identify internal structures and choose potential target sites for U–Pb analyses.

U–Pb dating analyses were conducted by LA-ICP-MS at Beijing Createch Testing Technology Comp. Ltd. Detailed operating conditions for the laser ablation system and the ICP-MS instrument and data reduction are the same as described by Hou et al. (2009). Laser sampling was performed using a RESOLUTION 193 nm laser ablation system. An Agilent 7500 ICP-MS instrument was used to acquire ion-signal intensities. Helium (with 5 ml/s of flow) was applied as a carrier gas from the sample chamber to the analyzer. The laser ablation spot

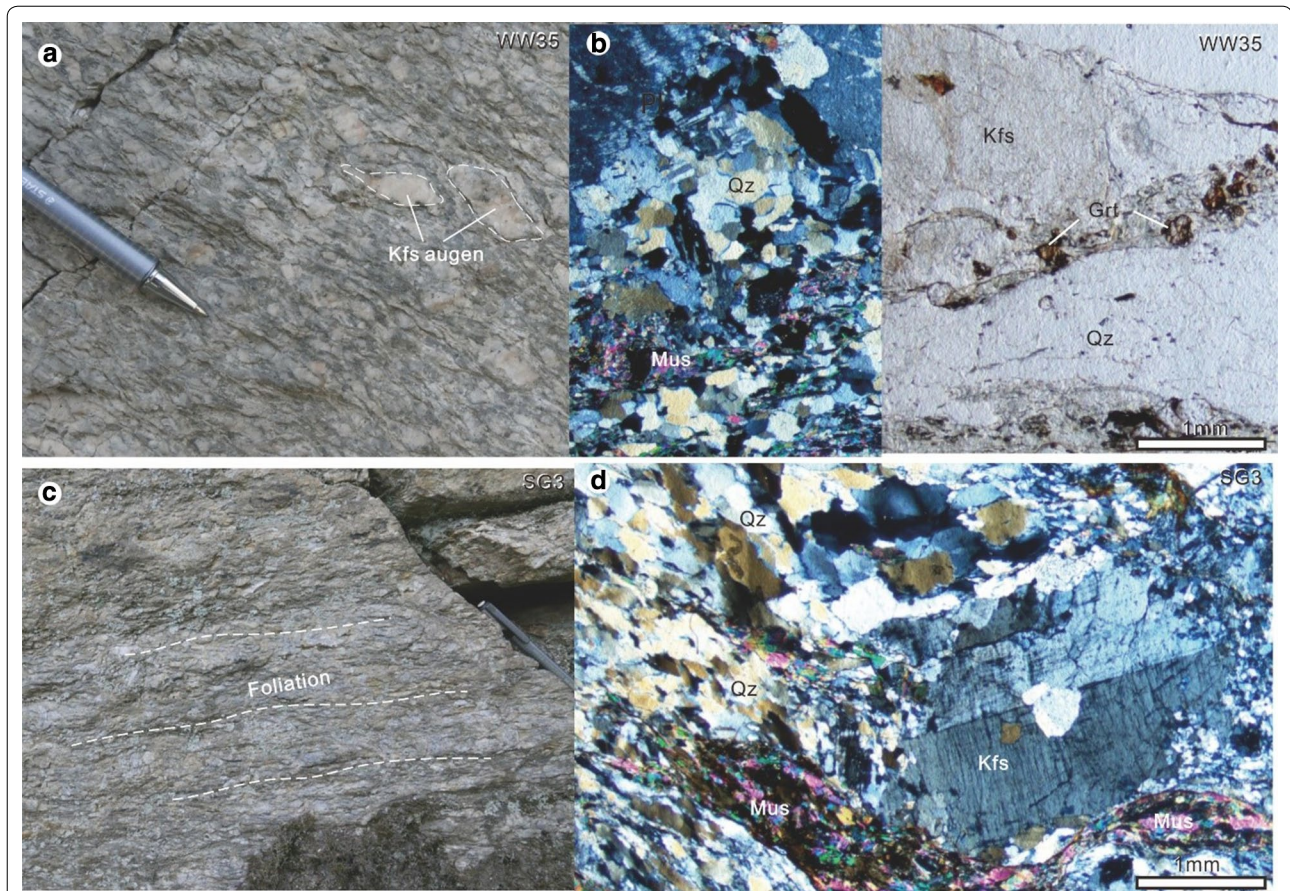


Fig. 3 Outcrop photos (**a**, **c**) of sample locations and representative photomicrographs (**b**, **d**) from the Grobneis (sample numbers are shown in the upper right corner). **a** Typical porphyritic texture of the Grobneis; **b** Photomicrographs both in plane-polarized light (right) and in cross-polarized light (left); **c** mylonitic fabric showing the moderate foliation; **d** lath-shaped K-feldspar (Kfs) displaying the Carlsbad twin in cross-polarized light. Qz, quartz; Kfs, potassium feldspar; Pl, plagioclase; Mus, muscovite; Grt, garnet

diameter was 32 μm with a repetition rate of 10 Hz and energy of 4 J/cm^2 . Each analysis incorporated a background acquisition of approximately 15–20 s (gas blank) followed by 45 s data acquisition from the sample. $^{206}\text{Pb}/^{207}\text{Pb}$, $^{206}\text{Pb}/^{238}\text{U}$, $^{206}\text{Pb}/^{235}\text{U}$ and $^{208}\text{Pb}/^{232}\text{Th}$ ratios were corrected using zircon 91500 as an external standard for both instrumental mass bias and elemental and isotopic fractionation. Zircon GJ-1 was used as external standard for U–Pb dating and was analyzed twice every 5–10 analyses. Time-dependent drifts of U–Th–Pb isotopic ratios were corrected using a linear interpolation (with time) for every 5–10 analyses according to the variations of GJ-1 (i.e., 2 zircon GJ-1 + 5–10 samples + 2 zircon GJ-1) (Liu et al. 2010). Uncertainty of preferred values for the external standard GJ-1 (with an age of 599.6 ± 2.9 Ma) was propagated to the ultimate results of the samples. Off-line raw data selection and subtraction of backgrounds and analytical signals, and time-drift correction and quantitative calibration for U–Pb dating

was performed by *ICPMSDataCal* (Liu et al. 2010). In all analyzed zircon grains the common Pb correction was not necessary due to the low signal of common ^{204}Pb and high $^{206}\text{Pb}/^{204}\text{Pb}$ ratio. Concordia diagrams and weighted mean calculations were made using *Isoplot/Ex_ver3* (Ludwig 2003).

U, Th and Pb and other zircon trace element compositions were calibrated by NIST 610 as an external standard. NIST 610 standards have been analysed in the same batch as the ages. The age and REE were analyzed at same time in one spot. Zircon trace element composition was calibrated using ^{29}Si as an internal standard and NIST610 as an external standard. The detailed analytical procedure of trace elements determinations can be found in Liu et al. (2007, 2008).

4.2 Zircon Lu–Hf isotopic analyses

In-situ zircon Hf isotope analyses were performed on the same zircon grains that were subjected to U–Pb dating,

at the Beijing Createch Testing Technology Co., Ltd, China, using a RESOLUTION SE 193 nm laser-ablation system attached to a Thermo Fisher Scientific Neptune Plus MC-ICP-MS. Instrumental conditions and data acquisition protocols were described by Hou et al. (2007). A stationary spot with a beam diameter of $\sim 38 \mu\text{m}$ has been used. As the carrier gas, Helium, was used to transport the ablated sample aerosol mixed with Argon from the laser-ablation cell to the MC-ICP-MS torch by a mixing chamber. A recommended $^{175}\text{Lu}/^{176}\text{Lu}$ ratio of 0.02655 was used for elemental fractionation (Xie et al. 2008). Yb isobaric interference on ^{176}Hf was corrected following the methods of Lizuka and Hirata (2005). GJ-1 standard yielded a mean $^{176}\text{Hf}/^{177}\text{Hf}$ ratio of 0.281990 ± 24 (2σ , $n=32$), which is consistent with the standard reference value of 0.282000 within error (Morel et al. 2008). A decay constant for ^{176}Lu of 1.867×10^{-11} (Söderlund et al. 2004) and present-day chondritic ratios of $^{176}\text{Hf}/^{177}\text{Hf}=0.282785$ and $^{176}\text{Lu}/^{177}\text{Hf}=0.0336$ (Bouvier et al. 2008) were adopted to calculate the $\epsilon\text{Hf}(t)$ values. GJ-1 was used as the primary standard for acquisition also for Hf isotopic data, 91500 as the secondary standard. $\epsilon\text{Hf}(t)$ values and Hf model ages were calculated using the methods of Bouvier et al. (2008) and Griffin et al. (2002), respectively.

4.3 Whole-rock geochemical analysis

Whole-rock major and trace element compositions were determined by X-ray fluorescence (XRF-1800; Shimadzu) on glass discs fused with lithium tetraborate and inductively coupled plasma mass spectrometry (Agilent 7500ce) at Beijing Createch Test Technology Co. Ltd., too. Prior to analysis, all samples were trimmed to remove weathered surfaces before being cleaned with deionized water and crushed to 200 mesh in an agate mill. Sample powders (~ 40 mg) were digested using HNO_3 and HF acids in Teflon bombs. Loss-on-ignition (LOI) values were measured after heating 1 g of sample in a furnace at 1000°C for several hours in a muffle furnace. The precision of the XRF analyses is within $\pm 2\%$ for the oxides greater than 0.5 wt% and within $\pm 5\%$ for the oxides greater than 0.1 wt%.

For trace element determinations, sample powders (about 50 mg) were dissolved in Teflon bombs using a HF + HNO_3 mixture for 48 h at about 190°C . The solution was evaporated to incipient dryness, dissolved by concentrated HNO_3 and evaporated at 150°C to dispel the fluorides. After being redissolved in 30% HNO_3 overnight, the samples were diluted to about 100 g for analysis. An internal standard solution containing the element Rh was used to monitor signal drift during analysis. Analytical results for USGS standards for ICP-MS (Jochum et al. 2005), the USGS reference glasses

GSA-1G, GSC-1G, GSD-1G, GSE-1G, BCR-2G, BHVO-2G and BIR-1G were investigated by different analytical techniques. Trace element data obtained from the different analytical techniques agreed within an uncertainty of 1–5%, indicating that the results between different methods are similar. Therefore, the preliminary working values for the four USGS GS glasses calculated from these data have a low level of uncertainty.

5 Results

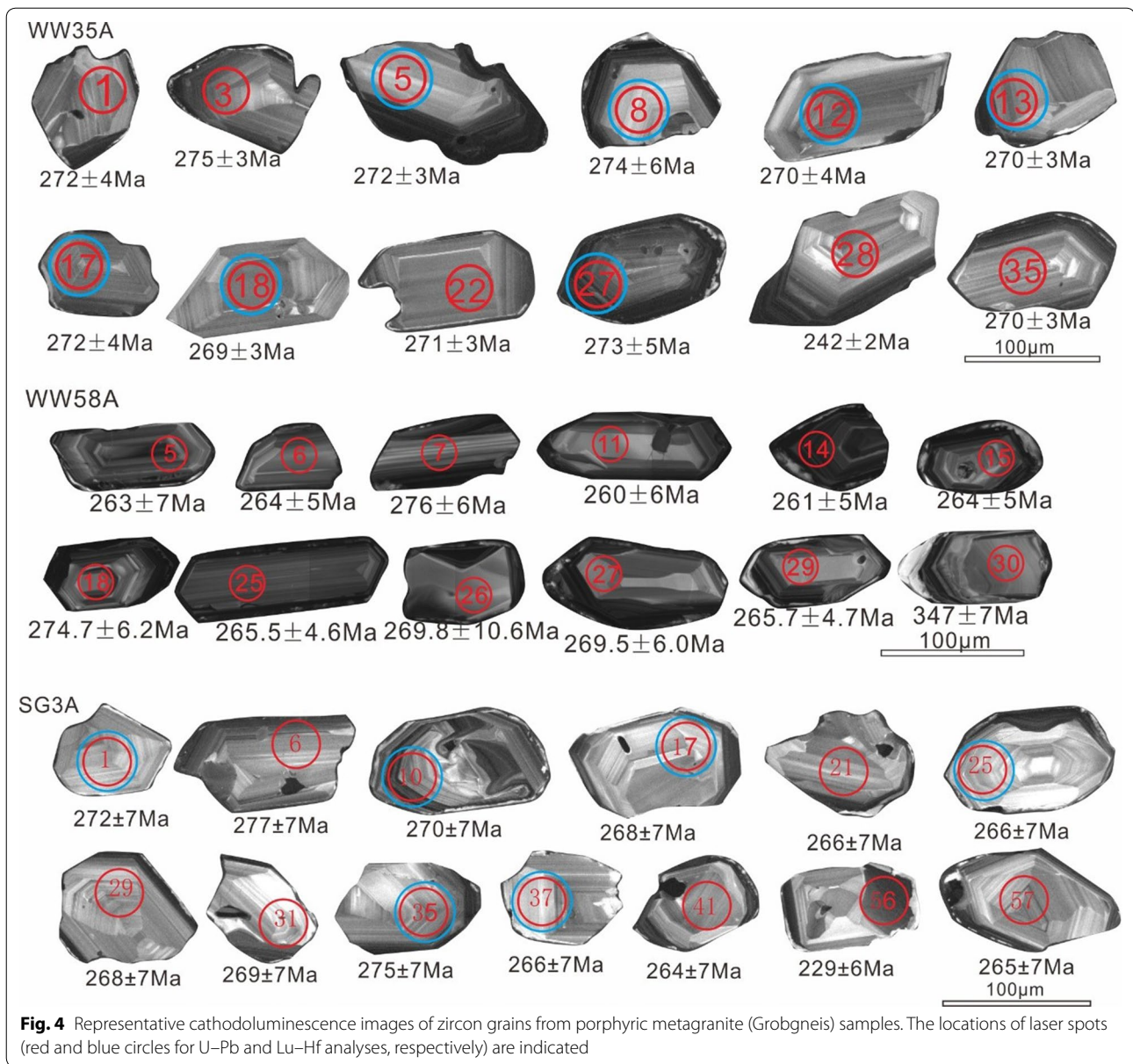
5.1 Zircon U–Pb dating

Three samples were prepared for zircon U–Pb dating analysis from porphyric metagranites. The representative zircon CL images of each sample are shown in Fig. 4. The zircon U–Pb dating results are listed in Table 1 and plotted in Fig. 5.

Zircons from sample WW35A are mainly euhedral and prismatic (80–160 μm), with aspect ratios of 2:1 to 4:1. The CL images of these zircons display that most of them have clear oscillatory zoning (Fig. 5a). Forty zircon grains were analyzed. Their Th/U ratios range between 0.11 and 0.87, supporting a magmatic origin. Thirty-four spots yield a lower intercept age of 272.0 ± 1.8 Ma and thirty-three concordant analyses yield a mean $^{206}\text{Pb}/^{238}\text{U}$ age of 272.2 ± 1.3 Ma (MSWD = 0.22) (Fig. 5a), which is considered to be the crystallization age of the granite intrusion. One inherited zircon grain with a distinct round core and narrow rim gives a $^{206}\text{Pb}/^{238}\text{U}$ age of 946 ± 12 Ma in the core. The younger Triassic age (mean $^{206}\text{Pb}/^{238}\text{U}$ age of 247.2 ± 8.6 Ma, $n=5$) is considered to represent the disturbing of later magmatic or metamorphic event (Table 1). The five zircons also display oscillatory zoning, their Th/U ratios range between 0.2 and 0.61.

The analyzed zircon grains from sample WW58A are colorless and/or pale, transparent, and commonly euhedral with sizes ranging from 50 to 140 μm and length to width ratios of 3:2 to 4:1. Most zircon grains show oscillatory zoning, some grains show a thin dark rim in CL images (Fig. 5b). The main group of zircons exhibit Th/U ratios ranging between 0.18 and 0.59, indicating that they are of magmatic origin. Sixteen analyses of U–Pb ages yield a mean $^{206}\text{Pb}/^{238}\text{U}$ age of 267.6 ± 2.9 Ma (MSWD = 0.63) and a concordia age of 267.5 ± 4.0 Ma (Fig. 5b). This age is interpreted as the crystallization age of the granite intrusion. Four zircons give Carboniferous and Early Permian ages indicating an earlier magmatic event. A grain has a Variscan age (346.8 ± 6.6 Ma), two zircon grains give pan-African ages (594 ± 16 , 627 ± 11 Ma), one grain has an age of 978 ± 17 Ma, other older, but discordant zircons show information on Early-Middle Proterozoic events.

Zircon crystals from sample SG3A are euhedral, transparent in color, with sizes ranging from 50 to



100 μm , and mainly rounded in shape except for a few prismatic zircon grains (Fig. 5c). The oscillatory growth zoning and relatively high Th/U ratios (mostly ~ 0.2 – 0.9) indicate their magmatic origin. We thus interpret this date as being the crystallization age of the granite. The ages of 51 zircon grains define a weighted mean $^{206}\text{Pb}/^{238}\text{U}$ age of 268.6 ± 2.3 Ma with an MSWD of 1.17 and an intercept age of 268.0 ± 2.3 Ma. Another group of ($n=7$) give a mean $^{206}\text{Pb}/^{238}\text{U}$ age of 230.9 ± 4.4 Ma (MSWD=0.47), measured on rims of both elongate and equant zircons, their Th/U ratios are very low typically for metamorphic zircons (Hoskin and Schaltegger 2003; Rubatto 2017) potentially indicating a Late

Triassic metamorphic overprint. Two inherited zircons (996 ± 25 Ma; 2029 ± 75 Ma) show similar ages with sample WW58A.

5.2 In situ Lu–Hf zircon isotopic compositions

In situ Lu–Hf zircon isotopic composition analysis was conducted on the representative middle Permian zircon grains from two samples dated by the zircon U–Pb method. Only magmatic zircon grains were analyzed. Therefore, initial Hf isotope compositions were calculated using the crystallization age determined for each sample (see Section 4.2). The results are presented in Table 2 and plotted in Fig. 6. The $^{176}\text{Hf}/^{177}\text{Hf}(t)$ ratios

Table 1 LA-ICP-MS zircon U–Pb data from porphyric metagranites (Grobgnais) of the Raabalpen basement

Spot	Isotope ratios					Rho	Ages	±σ						
	^{232}Th	^{238}U	$^{232}\text{Th}/^{238}\text{U}$	$^{207}\text{Pb}/^{206}\text{Pb}$	$^{207}\text{Pb}/^{235}\text{U}$			$^{206}\text{Pb}/^{238}\text{U}$	$^{207}\text{Pb}/^{206}\text{Pb}$	$^{207}\text{Pb}/^{235}\text{U}$	$^{206}\text{Pb}/^{238}\text{U}$			
WW35A: porphyric granite gneiss ("Grobgnais")														
1	216.36	484.44	0.45	0.05126	0.00054	0.30408	0.00064	0.98	254	24	270	4	272	4
2	247.32	482.69	0.51	0.05796	0.00137	0.34328	0.00814	0.68	528	57	300	6	272	4
3	177.18	759.08	0.23	0.05319	0.00101	0.32156	0.00880	0.46	345	44	283	7	275	3
4	104.67	301.10	0.35	0.05920	0.00140	0.34710	0.01199	0.76	576	57	303	9	269	7
5	135.98	359.05	0.38	0.05543	0.00122	0.32768	0.00670	0.61	432	45	288	5	272	3
6	222.47	256.57	0.87	0.07178	0.00070	1.56583	0.02688	0.79	989	19	957	11	946	12
7	249.35	485.10	0.51	0.05736	0.00119	0.34259	0.00977	0.37	506	46	299	7	272	3
8	115.63	1087.8	0.11	0.05669	0.00152	0.33822	0.00867	0.89	480	59	296	7	275	6
9	200.74	652.07	0.31	0.05163	0.00068	0.30936	0.00608	1.03	333	30	274	5	276	6
10	196.66	608.60	0.32	0.05869	0.00078	0.35426	0.00814	0.65	554	28	308	6	275	4
11	272.05	501.16	0.54	0.05312	0.00081	0.31608	0.00751	0.63	345	35	279	6	272	4
12	269.09	503.60	0.53	0.05648	0.00120	0.33595	0.01067	0.46	472	42	294	8	270	4
13	220.90	504.04	0.44	0.05227	0.00059	0.30991	0.00565	0.69	298	–5	274	4	271	3
14	188.05	348.53	0.54	0.05218	0.00105	0.28388	0.00774	0.68	295	42	254	6	249	5
15	287.25	449.09	0.64	0.05099	0.00065	0.30092	0.00568	0.65	239	62	267	4	270	3
16	221.32	360.37	0.61	0.06729	0.00247	0.35945	0.01849	0.33	856	76	312	14	242	4
17	290.99	542.92	0.54	0.05179	0.00058	0.30826	0.00616	0.81	276	26	273	5	272	4
18	354.83	693.09	0.51	0.05171	0.00064	0.30394	0.00487	0.77	272	30	270	4	269	3
19	274.63	382.41	0.72	0.06167	0.00222	0.36931	0.01605	0.28	663	78	319	12	272	3
20	182.31	368.80	0.49	0.05455	0.00078	0.32503	0.00614	0.72	395	36	286	5	273	4
21	291.94	478.44	0.61	0.05058	0.00062	0.30076	0.00555	0.78	220	28	267	4	272	4
22	285.53	397.67	0.72	0.05202	0.00077	0.30817	0.00533	0.71	287	33	273	4	271	3
23	365.45	555.15	0.66	0.05186	0.00064	0.30960	0.00518	0.84	280	28	274	4	273	4
24	349.60	583.33	0.60	0.05208	0.00076	0.31057	0.00601	0.70	287	33	275	5	272	4
25	428.18	766.60	0.56	0.05643	0.00090	0.33971	0.00744	0.58	478	35	297	6	274	3
26	437.84	1726.7	0.25	0.05086	0.00068	0.30449	0.00699	1.04	235	27	270	5	274	6
27	278.97	931.87	0.30	0.05097	0.00071	0.30457	0.00570	0.91	239	33	270	4	273	5
28	259.75	464.65	0.56	0.05074	0.00100	0.26883	0.00475	0.64	228	44	242	4	242	3
29	298.53	589.60	0.51	0.05053	0.00092	0.30308	0.00633	0.89	220	43	269	5	274	5
30	617.30	725.94	0.85	0.04989	0.00096	0.30346	0.00745	0.81	191	44	269	6	277	5
31	257.76	485.00	0.53	0.05326	0.00112	0.32356	0.00849	0.64	339	44	285	7	276	5
32	345.43	606.76	0.57	0.05173	0.00100	0.28678	0.00626	0.78	272	44	256	5	253	4
33	66.97	261.87	0.26	0.06267	0.00165	0.28124	0.00614	0.78	698	57	252	5	208	4

Table 1 (continued)

Spot	Isotope ratios										Rho		Ages			
	²³² Th	²³⁸ U	²³² Th/ ²³⁸ U	²⁰⁷ Pb/ ²⁰⁶ Pb	²⁰⁷ Pb/ ²³⁵ U	^{±σ}	²⁰⁶ Pb/ ²³⁸ U	^{±σ}	²⁰⁷ Pb/ ²⁰⁶ Pb	^{±σ}	²⁰⁷ Pb/ ²³⁵ U	^{±σ}	²⁰⁶ Pb/ ²³⁸ U	^{±σ}		
34	543.68	639.78	0.85	0.05072	0.00076	0.30226	0.00555	0.04308	0.00068	0.86	228	33	268	4	272	4
35	524.27	628.67	0.83	0.05244	0.00078	0.31173	0.00648	0.04280	0.00055	0.61	306	3	276	5	270	3
36	156.47	638.44	0.25	0.04968	0.00077	0.29890	0.00727	0.04353	0.00093	0.88	189	37	266	6	275	6
37	165.11	480.79	0.34	0.05325	0.00079	0.32125	0.00649	0.04357	0.00064	0.73	339	33	283	5	275	4
38	85.37	432.87	0.20	0.05129	0.00084	0.29119	0.00698	0.04104	0.00077	0.78	254	42	260	6	259	5
39	217.38	532.43	0.41	0.05216	0.00064	0.31222	0.00642	0.04334	0.00082	0.92	300	28	276	5	274	5
40	293.57	544.51	0.54	0.05726	0.00100	0.34248	0.00896	0.04305	0.00063	0.56	502	39	299	7	272	4
Spot	Isotope ratios										Ages					
²³² Th	²³⁸ U	²³² Th/ ²³⁸ U	²⁰⁷ Pb/ ²⁰⁶ Pb	²⁰⁷ Pb/ ²³⁵ U	^{±σ}	²⁰⁶ Pb/ ²³⁸ U	^{±σ}	²⁰⁷ Pb/ ²⁰⁶ Pb	^{±σ}	²⁰⁷ Pb/ ²³⁵ U	^{±σ}	²⁰⁶ Pb/ ²³⁸ U	^{±σ}			
WW58A: porphyric granite gneiss ("Grobgnéis")																
1	227.55	572.43	0.40	0.05216	0.00181		0.01256	0.03753	0.00102	0.21	254	24	270	4	272	4
2	170.27	171.94	0.99	0.12065	0.00198	4.40740	0.12608	0.26412	0.00562	0.65	528	57	300	6	272	4
3	99.13	201.56	0.49	0.11837	0.00222	4.92358	0.15206	0.30128	0.00811	0.91	345	44	283	7	275	3
4	103.25	1234.4	0.08	0.05385	0.00104	0.33401	0.00958	0.04498	0.00103	0.89	576	57	303	9	269	7
5	399.04	1253.2	0.32	0.05524	0.00102	0.31901	0.01145	0.04171	0.00119	0.87	432	45	288	5	272	3
6	234.78	460.73	0.51	0.05327	0.00116	0.30675	0.00867	0.04180	0.00087	0.70	989	19	957	11	946	12
7	162.60	407.83	0.40	0.05241	0.00138	0.31508	0.01039	0.04363	0.00097	0.66	506	46	299	7	272	3
8	287.81	244.40	Jan-18	0.07512	0.00106	1.69766	0.03715	0.16388	0.00315	0.91	480	59	296	7	275	6
9	80.55	2181.7	0.04	0.05463	0.00105	0.30744	0.01130	0.04087	0.00138	0.91	333	30	274	5	276	6
10	62.43	1414.5	0.04	0.05464	0.00094	0.30158	0.00875	0.03991	0.00086	0.99	554	28	308	6	275	4
11	120.40	664.68	0.18	0.05192	0.00092	0.29534	0.00812	0.04128	0.00096	0.85	345	35	279	6	272	4
12	33.44	1348.4	0.02	0.05169	0.00088	0.30865	0.00819	0.04324	0.00091	0.79	472	42	294	8	270	4
13	65.15	109.70	0.59	0.05562	0.00308	0.32254	0.02428	0.04145	0.00150	0.48	298	-5	274	4	271	3
14	599.68	1540.7	0.39	0.05242	0.00080	0.29939	0.00774	0.04128	0.00084	0.79	295	42	254	6	249	5
15	77.87	918.04	0.08	0.05098	0.00108	0.29303	0.00704	0.04185	0.00087	0.75	239	62	267	4	270	3
16	310.74	270.86	Jan-15	0.06236	0.00161	0.88090	0.02788	0.10219	0.00192	0.83	856	76	312	14	242	4
17	138.60	598.93	0.23	0.05310	0.00159	0.34666	0.01355	0.04729	0.00126	0.64	276	26	273	5	272	4
18	230.72	599.08	0.39	0.05346	0.00150	0.31923	0.00929	0.04354	0.00100	0.80	272	30	270	4	269	3
19	220.38	415.88	0.53	0.05840	0.00154	0.36954	0.00815	0.04620	0.00087	0.78	663	78	319	12	272	3
20	200.29	603.38	0.33	0.05256	0.00119	0.31210	0.01107	0.04273	0.00108	0.72	395	36	286	5	273	4
21	Sep-56	1089.8	0.01	0.06024	0.00092	0.80506	0.02563	0.09652	0.00273	0.94	220	28	267	4	272	4
22	131.86	526.16	0.25	0.05281	0.00142	0.33789	0.01048	0.04617	0.00066	0.46	287	33	273	4	271	3

Table 1 (continued)

Spot	Isotope ratios						Ages								
	^{232}Th	^{238}U	$^{232}\text{Th}/^{238}\text{U}$	$^{207}\text{Pb}/^{206}\text{Pb}$	$\pm\sigma$	$^{207}\text{Pb}/^{235}\text{U}$	$\pm\sigma$	$^{206}\text{Pb}/^{238}\text{U}$	$\pm\sigma$	$^{207}\text{Pb}/^{206}\text{Pb}$	($\pm\sigma$)	$^{206}\text{Pb}/^{238}\text{U}$	$\pm\sigma$		
23	133.10	373.15	0.36	0.04910	0.00120	0.28997	0.00785	0.04289	0.00081	0.66	280	274	4	273	4
24	227.51	694.26	0.33	0.05249	0.00141	0.30705	0.00858	0.04265	0.00096	0.78	287	275	5	272	4
25	371.18	714.07	0.52	0.05229	0.00096	0.30478	0.00826	0.04205	0.00075	0.61	478	297	6	274	3
26	158.12	374.72	0.42	0.05692	0.00194	0.33403	0.01633	0.04274	0.00172	0.81	235	270	5	274	6
27	184.20	477.10	0.39	0.05263	0.00141	0.30962	0.00991	0.04269	0.00097	0.72	239	270	4	273	5
28	475.57	1925.9	0.25	0.05274	0.00090	0.34776	0.01236	0.04758	0.00140	0.98	228	242	4	242	3
29	135.32	589.23	0.23	0.05422	0.00125	0.31512	0.00882	0.04208	0.00076	0.67	220	269	5	274	5
30	158.90	402.73	0.39	0.05314	0.00199	0.40411	0.01506	0.05527	0.00108	0.85	191	269	6	277	5
Spot	Isotope ratios						Ages								
^{232}Th	^{238}U	$^{232}\text{Th}/^{238}\text{U}$	$^{207}\text{Pb}/^{206}\text{Pb}$	$\pm\sigma$	$^{207}\text{Pb}/^{235}\text{U}$	$\pm\sigma$	$^{206}\text{Pb}/^{238}\text{U}$	$\pm\sigma$	$^{207}\text{Pb}/^{206}\text{Pb}$	($\pm\sigma$)	$^{206}\text{Pb}/^{238}\text{U}$	$\pm\sigma$			
1	287.21	393.07	0.73	0.05266	0.00152	0.31326	0.01028	0.04314	0.00114	0.9	314	277	8	272	7
2	424.38	625.9	0.68	0.052	0.00135	0.31023	0.00944	0.04326	0.00114	0.9	285	274	7	273	7
3	591.14	893.7	0.66	0.05373	0.00113	0.31182	0.00908	0.04208	0.0011	0.9	360	276	7	266	7
4	205.07	633.61	0.32	0.05204	0.0028	0.29778	0.01392	0.0415	0.0011	0.89	287	265	11	262	7
5	72.53	457.63	0.16	0.05208	0.00252	0.30469	0.01239	0.04243	0.00111	0.89	289	270	10	268	7
6	215.9	391.18	0.55	0.05566	0.00159	0.337	0.01095	0.0439	0.00116	0.9	439	295	8	277	7
7	199.57	439.71	0.45	0.05357	0.0015	0.32071	0.01029	0.04341	0.00115	0.9	353	282	8	274	7
8	152.38	391.66	0.39	0.07129	0.00158	1.59005	0.0437	0.16174	0.00421	0.9	966	966	17	966	23
9	247.48	675.75	0.37	0.05238	0.00345	0.29003	0.0174	0.04016	0.00109	0.88	302	259	14	254	7
10	343.1	836.03	0.41	0.05058	0.00125	0.29785	0.00878	0.0427	0.00112	0.9	222	265	7	270	7
11	103.06	2400.9	0.04	0.05028	0.00204	0.25489	0.00809	0.03677	0.00094	0.88	208	231	7	233	6
12	352.9	501.83	0.70	0.05536	0.00163	0.30395	0.01011	0.03981	0.00106	0.9	427	269	8	252	7
13	105.47	648.41	0.16	0.0504	0.0013	0.30222	0.00918	0.04348	0.00114	0.9	213	268	7	274	7
14	201.56	456.04	0.44	0.05126	0.00138	0.30103	0.00941	0.04259	0.00112	0.9	253	267	7	269	7
15	300.11	546.15	0.55	0.05225	0.00139	0.3116	0.00964	0.04325	0.00114	0.9	296	275	7	273	7
16	91.03	275.8	0.33	0.05273	0.00165	0.33287	0.01159	0.04578	0.00122	0.9	317	292	9	289	8
17	176.56	516.25	0.34	0.0539	0.00307	0.31587	0.01589	0.0425	0.00114	0.89	367	279	12	268	7
18	224.93	470.39	0.48	0.05394	0.00147	0.31288	0.00982	0.04206	0.00111	0.9	369	276	8	266	7
19	115.44	280.14	0.41	0.05254	0.00383	0.3037	0.02049	0.04193	0.00116	0.87	309	269	16	265	7
20	169.87	451.36	0.38	0.0524	0.00145	0.30763	0.0098	0.04257	0.00112	0.9	303	272	8	269	7
21	269.72	663.78	0.41	0.05268	0.00135	0.3066	0.00925	0.0422	0.00111	0.9	315	272	7	266	7

SG3A; porphyric granite gneiss ("Grobgnais")

Table 1 (continued)

Spot	Isotope ratios										Ages					
	²³² Th	²³⁸ U	²³² Th/ ²³⁸ U	²⁰⁷ Pb/ ²⁰⁶ Pb	$\pm\sigma$	²⁰⁷ Pb/ ²³⁵ U	$\pm\sigma$	²⁰⁶ Pb/ ²³⁸ U	$\pm\sigma$	²⁰⁷ Pb/ ²⁰⁶ Pb	$\pm\sigma$	²⁰⁷ Pb/ ²³⁵ U	$\pm\sigma$	²⁰⁶ Pb/ ²³⁸ U	$\pm\sigma$	
22	191.4	419.56	0.46	0.0521	0.00148	0.30511	0.00988	0.04246	0.00112	0.9	290	34	270	8	268	7
23	2068.3	1845.0	01-Dec	0.05209	0.00117	0.25751	0.00715	0.03584	0.00093	0.9	289	28	233	6	227	6
24	282.16	918.12	0.31	0.12499	0.00518	5.31215	0.17043	0.30824	0.00808	0.91	2029	75	1871	27	1732	40
25	174.67	561.38	0.31	0.05063	0.00134	0.29422	0.00908	0.04214	0.00111	0.9	224	32	262	7	266	7
26	260.73	449.48	0.58	0.05468	0.00159	0.33349	0.01098	0.04422	0.00117	0.9	399	34	292	8	279	7
27	282.08	564.16	0.50	0.05488	0.00142	0.33394	0.01013	0.04412	0.00116	0.9	407	30	293	8	278	7
28	123.11	223.89	0.55	0.05223	0.00176	0.30992	0.0114	0.04303	0.00116	0.9	295	40	274	9	272	7
29	279.82	490.04	0.57	0.05441	0.00144	0.31811	0.0098	0.0424	0.00112	0.9	388	31	280	8	268	7
30	169.59	1720.9	0.10	0.05022	0.0021	0.27379	0.00908	0.03954	0.00101	0.9	205	99	246	7	250	6
31	105.21	393.92	0.27	0.05548	0.00157	0.32556	0.01049	0.04255	0.00113	0.9	432	33	286	8	269	7
32	159.5	281.75	0.57	0.05096	0.00162	0.3036	0.01068	0.0432	0.00115	0.9	239	38	269	8	273	7
33	171.59	498.95	0.34	0.05774	0.00166	0.35103	0.01147	0.04409	0.00117	0.9	520	33	305	9	278	7
34	198.76	541.13	0.37	0.05145	0.00138	0.30306	0.00941	0.04272	0.00112	0.9	261	32	269	7	270	7
35	228.13	879.55	0.26	0.05312	0.0028	0.31961	0.01459	0.04364	0.00115	0.89	334	123	282	11	275	7
36	28.77	1537.8	0.02	0.05161	0.00116	0.26019	0.00721	0.03656	0.00095	0.9	268	28	235	6	231	6
37	523.81	579.01	0.90	0.05064	0.00134	0.29462	0.00908	0.04219	0.00111	0.9	224	32	262	7	266	7
38	676.21	815.52	0.83	0.05116	0.00127	0.29193	0.0086	0.04138	0.00108	0.9	248	30	260	7	261	7
39	164.25	590.69	0.28	0.0527	0.00137	0.31252	0.00949	0.04301	0.00113	0.9	316	31	276	7	271	7
40	230.11	706.53	0.33	0.05132	0.00129	0.30281	0.009	0.04279	0.00112	0.9	255	31	269	7	270	7
41	489.17	861.22	0.57	0.05326	0.00371	0.30715	0.01969	0.04183	0.00115	0.88	340	161	272	15	264	7
42	187.3	506.56	0.37	0.05115	0.00138	0.30859	0.00961	0.04375	0.00115	0.9	248	32	273	7	276	7
43	238.46	579.71	0.41	0.05333	0.00137	0.33351	0.01007	0.04535	0.00119	0.9	343	31	292	8	286	7
44	146.93	2174.3	0.07	0.05208	0.00114	0.2713	0.0074	0.03778	0.00098	0.9	289	28	244	6	239	6
45	219.4	485.41	0.45	0.05198	0.00142	0.30304	0.00953	0.04228	0.00111	0.9	285	32	269	7	267	7
46	149.9	405.88	0.37	0.05142	0.00145	0.3133	0.0101	0.04418	0.00117	0.9	260	34	277	8	279	7
47	100.83	312.97	0.32	0.05298	0.00161	0.30887	0.01052	0.04228	0.00112	0.9	328	36	273	8	267	7
48	42.89	2466.1	0.02	0.05187	0.00114	0.25925	0.00706	0.03624	0.00094	0.9	280	28	234	6	229	6
49	130.62	556.02	0.23	0.0548	0.00145	0.31657	0.00973	0.04189	0.0011	0.9	404	31	279	8	265	7
50	502.24	728.25	0.69	0.05429	0.00135	0.31431	0.00926	0.04198	0.0011	0.9	383	30	278	7	265	7
51	308.13	561.87	0.55	0.05702	0.00158	0.33676	0.01069	0.04283	0.00113	0.9	492	32	295	8	270	7
52	173.29	427.93	0.40	0.05092	0.00144	0.29155	0.00939	0.04152	0.0011	0.9	237	34	260	7	262	7
53	414.12	632.33	0.65	0.05577	0.00152	0.33884	0.01063	0.04406	0.00116	0.9	443	31	296	8	278	7
54	276.68	618.42	0.45	0.05111	0.00132	0.29058	0.00882	0.04123	0.00108	0.9	246	31	259	7	260	7

Table 1 (continued)

Spot	Isotope ratios					Ages										
	^{232}Th	^{238}U	$^{232}\text{Th}/^{238}\text{U}$	$^{207}\text{Pb}/^{206}\text{Pb}$	$\pm\sigma$	$^{207}\text{Pb}/^{235}\text{U}$	$\pm\sigma$	$^{206}\text{Pb}/^{238}\text{U}$	$\pm\sigma$	$^{207}\text{Pb}/^{206}\text{Pb}$	$\pm\sigma$	$^{206}\text{Pb}/^{238}\text{U}$	$\pm\sigma$			
55	274.84	517.53	0.53	0.05144	0.00138	0.29877	0.00928	0.04212	0.00111	0.9	261	32	265	7	266	7
56	08-May	2298.3	0.00	0.05162	0.00189	0.25754	0.00682	0.03619	0.00091	0.88	269	86	233	6	229	6
57	618.33	663.54	0.93	0.04976	0.00128	0.28758	0.00867	0.04191	0.0011	0.9	184	31	257	7	265	7
58	495.48	621.32	0.80	0.05159	0.00134	0.29089	0.00884	0.04089	0.00107	0.9	267	31	259	7	258	7
59	496.01	743.17	0.67	0.05173	0.00129	0.29534	0.00872	0.0414	0.00108	0.9	273	30	263	7	262	7
60	109.53	2972.0	0.04	0.05074	0.00192	0.25194	0.00704	0.03601	0.00092	0.89	229	89	228	6	228	6

of magmatic zircons from sample WW35A range from 0.282500 to 0.2826073, corresponding to $\epsilon\text{Hf}(t)$ of -4.2 to -0.6 (Fig. 6 and Table 2), and the corresponding crustal model ages range from 1.31 Ga to 1.54 Ga. Sample SG3A shows a tighter range of zircon $^{176}\text{Hf}/^{177}\text{Hf}(t)$, from 0.282499 to 0.282563 equivalent to $\epsilon\text{Hf}(t)$ of -4.54 to -2.34 , and the corresponding crustal model ages range from 1.43 to 1.56 Ga (Fig. 6 and Table 2).

5.3 Whole-rock major and trace element data

Whole-rock major and trace element compositions of the representative samples are listed in Table 3. All samples plot into the granite field, near the boundary of quartz-syenite and granite field of the total alkalis-silica (TAS) diagram (Fig. 7a).

All samples have high SiO_2 (69.83–72.55 wt%), $\text{Na}_2\text{O} + \text{K}_2\text{O}$ (8.24–9.88 wt%), K_2O contents (4.60–6.25 wt%) with $\text{K}_2\text{O}/\text{Na}_2\text{O}$ ratios from 1.20 to 1.79 and high normative corundum (1.24–1.90%), displaying a trend of high-K calc-alkaline to shoshonitic series (Fig. 7b and c). Their A/CNK ($\text{Al}_2\text{O}_3/(\text{CaO} + \text{Na}_2\text{O} + \text{K}_2\text{O})$ mol.) and A/NK ($\text{Al}_2\text{O}_3/(\text{Na}_2\text{O} + \text{K}_2\text{O})$ mol.) ratios range from 1.11 to 1.19, and from 1.26 to 1.35, respectively, are similar to those of S-type granite (Fig. 7d). In addition, the samples show low contents of TiO_2 (0.19–0.26 wt%), $\text{Fe}_2\text{O}_3\text{t}$ (1.59–2.10 wt%), CaO (0.62–1.03 wt%) and MgO (0.33–0.51 wt%).

In the chondrite-normalized REE distribution patterns, the samples exhibit enrichment of LREE and moderately negative Eu anomalies ($\delta\text{Eu} = 0.28\text{--}0.81$) (Fig. 8a) with LREE/HREE and $(\text{La}/\text{Yb})_N$ ratios varying from 2.66 to 4.40, and 7.61 to 13.77, respectively. All samples show negative anomalies of Ba, Nb, Sr and Ti, and positive anomalies of Cs, Rb, Th and U in the primitive mantle-normalized multi-element variation diagram (Fig. 8b).

6 Discussion

6.1 Age of the porphyric metagranites (Grobgnais)

This LA-ICP-MS zircon U–Pb study of porphyric metagranites from three widely spaced localities within the Raabalpen basement of the Lower Austroalpine unit has complemented an ambiguous question about the age and origin of these rocks. Considering the age and composition of the studied samples and the wide distribution of similar coeval volcanic rocks (Permian porphyroids, Fig. 2) in the Lower Austroalpine unit, it is now evident that the porphyric metagranites are part of a large Middle Permian granitoid belt, extending from the Western Alps through the Eastern Alps to the Western Carpathians.

The dated porphyric metagranites with ages of 272.2 ± 1.3 Ma, 267.7 ± 2.9 Ma, 268.6 ± 2.3 Ma, are much

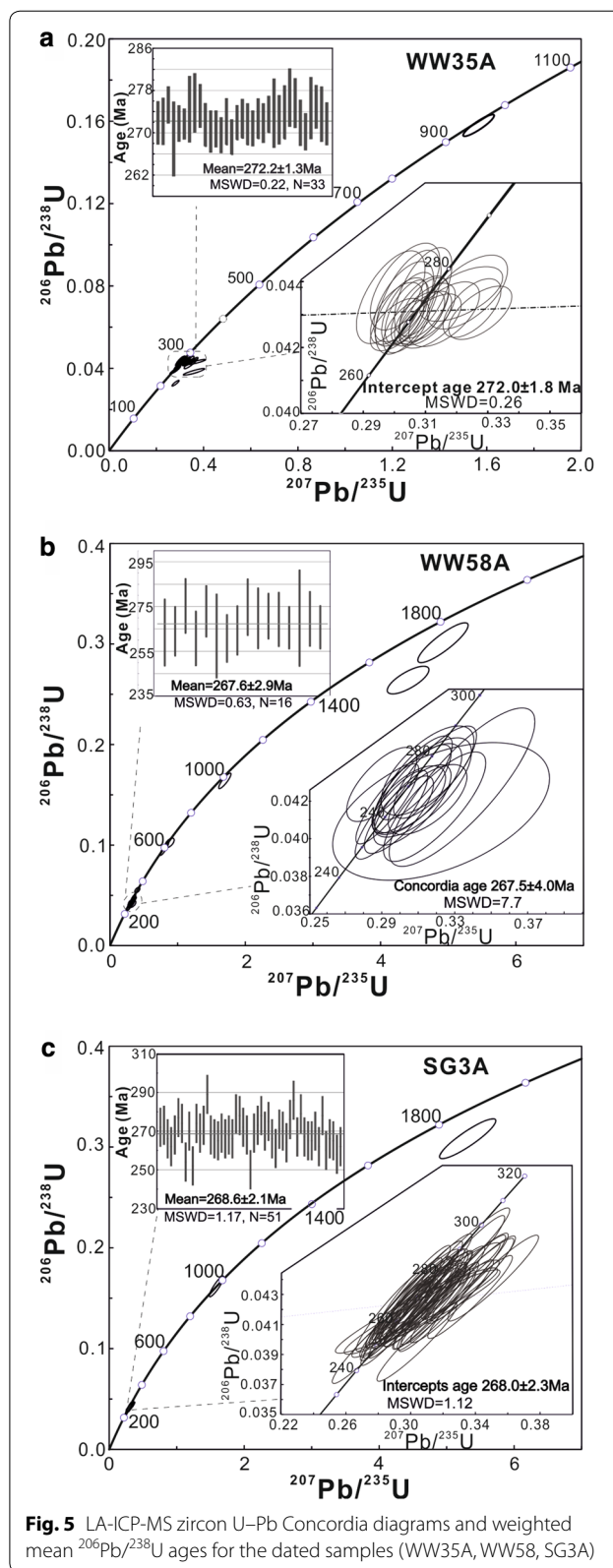
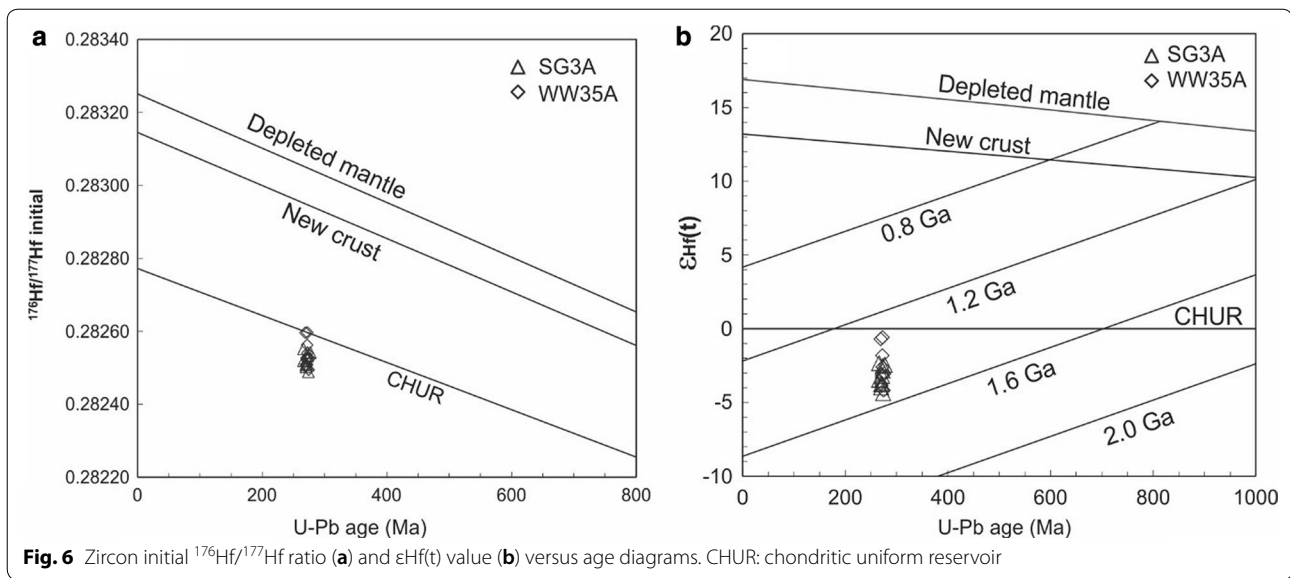


Fig. 5 LA-ICP-MS zircon U–Pb Concordia diagrams and weighted mean $^{206}\text{Pb}/^{238}\text{U}$ ages for the dated samples (WW35A, WW58, SG3A)

Table 2 Hf isotopic data of zircons from porphyric metagranites (Grobneis) in the Raabalpen basement

Sample No.	Age (Ma)	$^{176}\text{Yb}/^{177}\text{Hf}$	2σ	$^{176}\text{Lu}/^{177}\text{Hf}$	2σ	$^{176}\text{Hf}/^{177}\text{Hf}$	2σ	$^{176}\text{Hf}/^{177}\text{Hf}_i$	$e_{\text{Hf}}(0)$	$e_{\text{Hf}}(t)$	$e_{\text{Hf}}(t)'$	2σ	T_{DM} (Ma)	T_{DM}^{C} (Ma)	$f_{\text{Lu/Hf}}$
WW35-1	272	0.042149	0.000406	0.001474	0.000015	0.282531	0.000018	0.282523	-8.5	-2.8	-2.2	0.7	1034	1472	-0.96
WW35-2	274	0.033139	0.000203	0.001163	0.000005	0.282500	0.000019	0.282494	-9.6	-3.8	-3.1	0.7	1069	1536	-0.96
WW35-3	276	0.071474	0.000298	0.002361	0.000008	0.282538	0.000019	0.282525	-8.3	-2.7	-2.0	0.7	1050	1464	-0.93
WW35-4	270	0.05111	0.000504	0.001708	0.000017	0.282518	0.000019	0.282509	-9.0	-3.4	-2.7	0.7	1060	1505	-0.95
WW35-5	271	0.073485	0.002628	0.002460	0.000092	0.282517	0.000018	0.282505	-9.0	-3.5	-2.8	0.7	1082	1513	-0.93
WW35-6	272	0.058853	0.000702	0.001956	0.000020	0.282572	0.000020	0.282562	-7.1	-1.4	-0.7	0.7	988	1384	-0.94
WW35-7	269	0.042783	0.000277	0.001485	0.000014	0.282603	0.000024	0.282596	-6.0	-0.3	0.5	0.8	931	1310	-0.96
WW35-8	273	0.052678	0.001634	0.001751	0.000050	0.282549	0.000020	0.28254	-7.9	-2.2	-1.5	0.7	1016	1433	-0.95
WW35-9	272	0.052471	0.000837	0.001751	0.000023	0.282536	0.000017	0.282527	-8.3	-2.7	-2.1	0.6	1034	1463	-0.95
WW35-10	272	0.060763	0.000331	0.002084	0.000012	0.282607	0.000020	0.282597	-5.8	-0.2	0.5	0.7	941	1307	-0.94
SG3-1	272	0.051970	0.000686	0.001715	0.000026	0.282532	0.000015	0.282523	-8.5	-2.8	-2.3	0.5	1039	1472	-0.95
SG3-2	273	0.054105	0.001062	0.001769	0.000038	0.282542	0.000014	0.282533	-8.1	-2.5	-2.0	0.5	1026	1449	-0.95
SG3-3	266	0.062724	0.000922	0.002026	0.000031	0.282530	0.000015	0.282520	-8.6	-3.1	-6	0.5	1051	1483	-0.94
SG3-4	270	0.063126	0.000415	0.002134	0.000008	0.282513	0.000012	0.282502	-9.2	-3.6	-3.2	0.4	1079	1520	-0.94
SG3-5	268	0.053446	0.000605	0.001749	0.000021	0.282518	0.000018	0.282509	-9.0	-3.4	-2.8	0.6	1061	1506	-0.95
SG3-6	266	0.068914	0.000508	0.002328	0.000016	0.282563	0.000017	0.282552	-7.4	-2.0	-1.4	0.6	1011	1412	-0.93
SG3-7	272	0.056644	0.000786	0.001865	0.000023	0.282518	0.000018	0.282508	-9.0	-3.4	-2.7	0.6	1064	1505	-0.94
SG3-8	273	0.038264	0.000805	0.001288	0.000029	0.282548	0.000015	0.282542	-7.9	-2.1	-1.6	0.5	1004	1429	-0.96
SG3-9	275	0.053560	0.000322	0.001778	0.000006	0.282551	0.000015	0.282542	-7.8	-2.1	-1.6	0.5	1014	1429	-0.95
SG3-10	266	0.060666	0.000493	0.001985	0.000015	0.282499	0.000016	0.282490	-9.6	-4.2	-3.6	0.6	1094	1551	-0.94



younger than previously assumed. Indeed, on geological grounds, the metagranite protoliths previously have been assigned to Carboniferous (Neubauer et al. 1992 and references therein). Similar Permian ages from a porphyric metagranite (271 ± 7 Ma) and from a leucophyllite (271 ± 6 Ma) were reported from the Miesenbach valley (2 km NE of Birkfeld, Fig. 2) (Chen et al. 2020) in the same unit. These geochronological data reveal that the porphyric metagranite in the Lower Austroalpine unit was emplaced in Middle Permian. The age is the same within error as the 264 ± 7 Ma-age of an associated gabbro determined by the Sm–Nd method (Schuster et al. 2001b). These gabbros represent only a very small volume but indicate bimodal magmatism.

Although occurring in few zircon, one sample give a pan-African event from inherited zircon, another few grains in all samples give the Early and Middle Proterozoic information. Those inherited zircons potentially indicate the protolith ages. A few of the igneous zircons from sample WW58 give the Carboniferous and Early Permian ages, those zircons interestingly correspond to the Rb–Sr whole-rock isochrone of 338 ± 12 Ma (Neubauer et al. 1992; Schermaier et al. 1997 and references therein). The source of Grobgnais-type porphyric metagranites probably is derived from the partial melting of paragneiss and schist in the Raabalpen basement. Additionally, the three samples also include variable Triassic ages. Rb–Sr ages of white mica from the granite yield cooling ages of 231 Ma (Tropper et al. 2007), which correspond to a zircon age population of ~ 230.9 Ma, it indicates that a Middle Triassic tectonothermal event exist in the Lower Austroalpine unit. We explain it to correspond to the second extensional event in Eastern

Alps, which finally led to the opening of the oceanic Meliata basin (Neubauer et al. 2018).

6.2 Origin and source nature of the Grobgnais porphyric metagranites

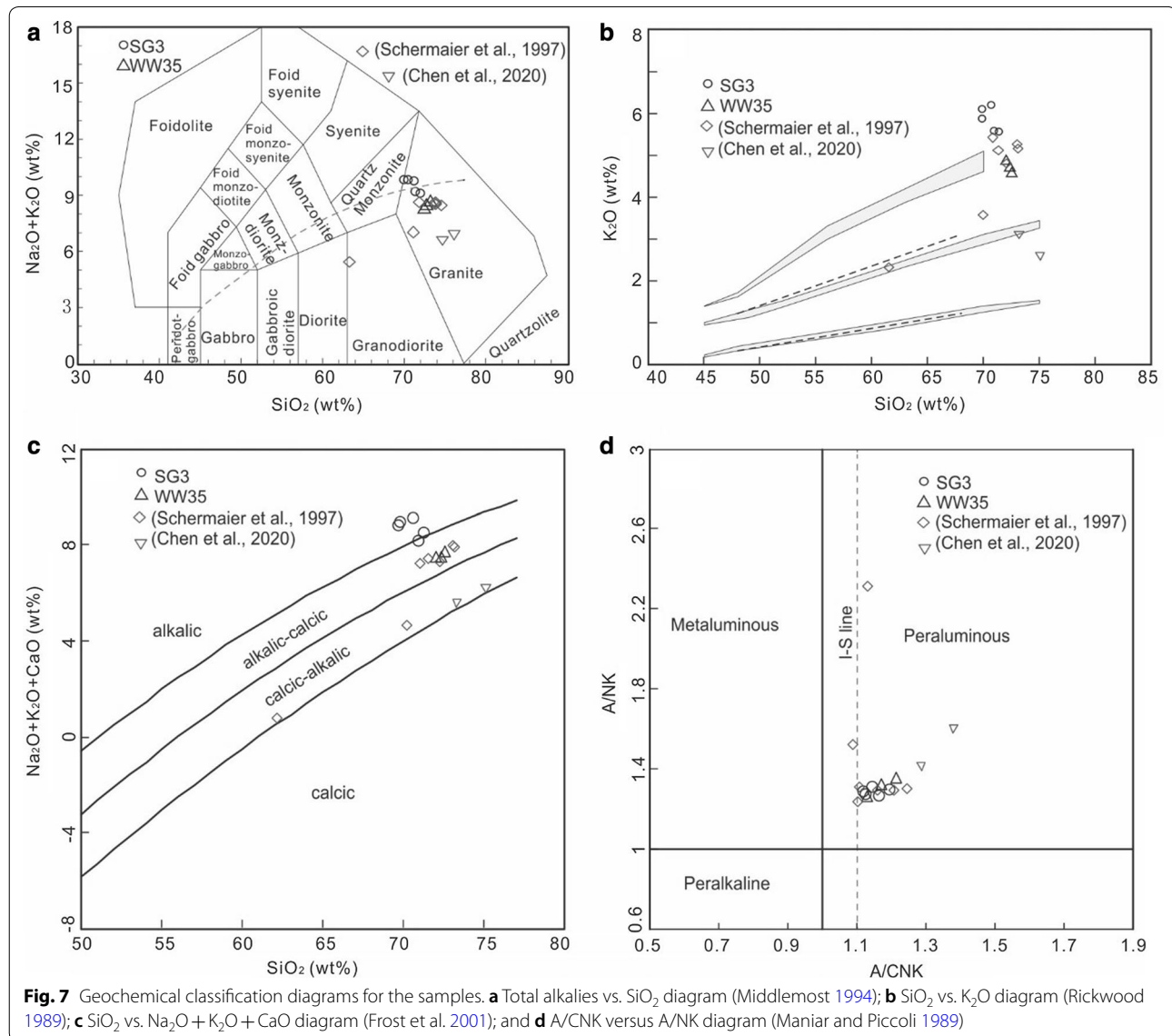
Grobgnais porphyric metagranites of the Lower Austroalpine unit are widespread, however, their origin and source still unclear. According to different magma sources and formation mechanisms, granitoids in the Earth's continental crust are genetically divided into M-, I-, S- and A-types (Bonin 2007; Chappell and White 2001; Frost et al. 2001). Grobgnais metagranites are composed of quartz, K-feldspar, plagioclase, muscovite, biotite, and garnet, lacking hornblende that is characteristic of I-type granite or aluminum-rich minerals that are characteristic of S-type granite (Chappell and White 1974; Miller 1985). In the $[\text{Zr} + \text{Nb} + \text{Ce} + \text{Y}]$ versus FeOt/MgO discrimination diagram (Fig. 9a), samples plot in the fields between fractionated and M-, I-, S-type granites. They further exhibit many S-type granite characteristics: (1) a strongly peraluminous character with high A/CNK values ranging from 1.11 to 1.19 (Fig. 7d), and relatively low CaO and Na_2O contents of 0.62–1.03 wt% and 3.36–3.85 wt%, respectively (Fig. 9b) corresponding to data of Schermaier et al. (1997), who interpreted the Grobgnais as Carboniferous S-type granite formed during Variscan plate collision. These geochemical characteristics are consistent with a derivation of the granites from a sedimentary source (Chappell 1999; Chappell and White 2001); (2) low Th and Y contents of 11.09–14.77 ppm and 14.38–22.90 ppm, respectively, both of which decrease with increasing Rb (Fig. 9c and d). This feature is frequently used as criterion to distinguish S-type

Table 3 Major (wt%), trace and rare earth element (ppm) analyses of porphyric metagranites (“Grobgneis”)

Sample	SG3A1	SG3A2	SG3B	SG3C	SG3D	WW35A	WW35B	WW35C
SiO ₂	70.58	69.83	71.29	69.83	70.97	72.36	72.55	72.06
TiO ₂	0.19	0.19	0.22	0.20	0.20	0.24	0.24	0.26
Al ₂ O ₃	15.82	16.33	15.31	16.24	15.45	14.43	14.26	14.59
Fe ₂ O ₃ T	1.59	1.63	1.86	1.67	1.78	1.94	1.90	2.10
MnO	0.03	0.03	0.03	0.03	0.04	0.04	0.04	0.03
MgO	0.33	0.34	0.40	0.34	0.38	0.46	0.43	0.51
CaO	0.65	1.03	0.62	1.00	0.99	0.86	0.86	0.79
Na ₂ O	3.50	3.74	3.50	3.85	3.50	3.56	3.83	3.36
K ₂ O	6.25	6.14	5.61	5.92	5.63	4.73	4.60	4.88
P ₂ O ₅	0.13	0.13	0.13	0.14	0.13	0.19	0.19	0.19
LOI	1.28	1.08	1.36	1.27	1.27	1.15	0.97	1.20
Total	100.36	100.47	100.33	100.50	100.32	99.96	99.88	99.96
A/CNK	1.15	1.11	1.18	1.12	1.13	1.15	1.11	1.19
A/NK	1.26	1.28	1.29	1.27	1.30	1.31	1.26	1.35
V	23.04	15.55	25.53	24.16	12.66	24.89	28.75	30.49
Cr	2.19	2.37	6.10	2.24	1.22	17.26	1.61	8.00
Co	2.53	2.29	3.01	1.98	2.46	2.34	2.67	2.92
Ni	43.55	25.02	56.16	9.71	27.67	10.98	34.10	24.56
Ga	18.40	19.70	19.19	19.33	18.90	18.44	16.99	19.50
Rb	240.00	251.52	227.90	233.11	222.44	251.05	240.38	276.59
Sr	89.07	106.24	76.45	100.41	89.62	65.01	65.34	63.91
Y	14.38	22.90	14.50	22.02	22.20	19.07	19.49	18.91
Zr	139.11	128.58	162.51	144.01	145.56	129.56	123.09	136.59
Nb	10.73	11.20	12.87	11.41	11.20	15.67	15.89	17.02
Cs	4.15	4.48	4.19	4.20	4.27	7.56	7.76	7.81
Ba	461.20	498.39	387.53	414.38	392.97	284.75	252.07	297.59
La	19.71	30.18	19.99	26.23	27.28	24.76	27.46	28.06
Ce	55.20	63.82	63.82	58.48	58.87	56.54	65.32	62.76
Pr	5.20	7.36	5.50	6.66	6.98	6.04	6.70	6.70
Nd	18.14	26.49	18.85	23.88	24.91	22.39	24.68	24.85
Sm	3.90	5.70	4.09	5.14	5.38	4.63	5.03	5.17
Eu	0.58	0.87	0.57	0.78	0.76	0.53	0.55	0.54
Gd	2.96	4.51	3.00	4.28	4.34	3.90	4.09	4.18
Tb	0.50	0.72	0.51	0.68	0.69	0.60	0.61	0.61
Dy	2.86	4.14	3.01	3.98	4.04	3.43	3.43	3.39
Ho	0.52	0.75	0.54	0.73	0.74	0.63	0.62	0.60
Er	1.52	2.15	1.59	2.09	2.12	1.81	1.73	1.64
Tm	0.23	0.31	0.24	0.30	0.30	0.25	0.24	0.22
Yb	1.57	1.97	1.63	1.96	1.94	1.61	1.57	1.43
Lu	0.22	0.27	0.23	0.27	0.27	0.23	0.21	0.19
Hf	3.80	3.49	4.44	3.88	3.92	3.61	3.41	3.70
Ta	1.00	1.01	1.16	1.05	1.02	1.82	1.86	1.92
Th	11.09	12.20	13.37	12.25	12.23	14.16	14.42	14.77
U	3.11	3.83	3.50	3.93	3.78	3.84	4.12	3.65
(La/Yb) _N	13.77	8.29	8.36	14.45	7.47	7.61	10.37	9.67
Eu/Eu*	0.59	0.59	0.81	0.75	0.28	0.67	0.75	0.70
ΣREE	113.11	149.26	123.57	135.45	138.63	127.34	142.24	140.36
M	1.30	1.38	1.26	1.37	1.32	1.26	1.31	1.22
T _{Zr}	782	770	799	780	785	779	771	786

Table 3 (continued)

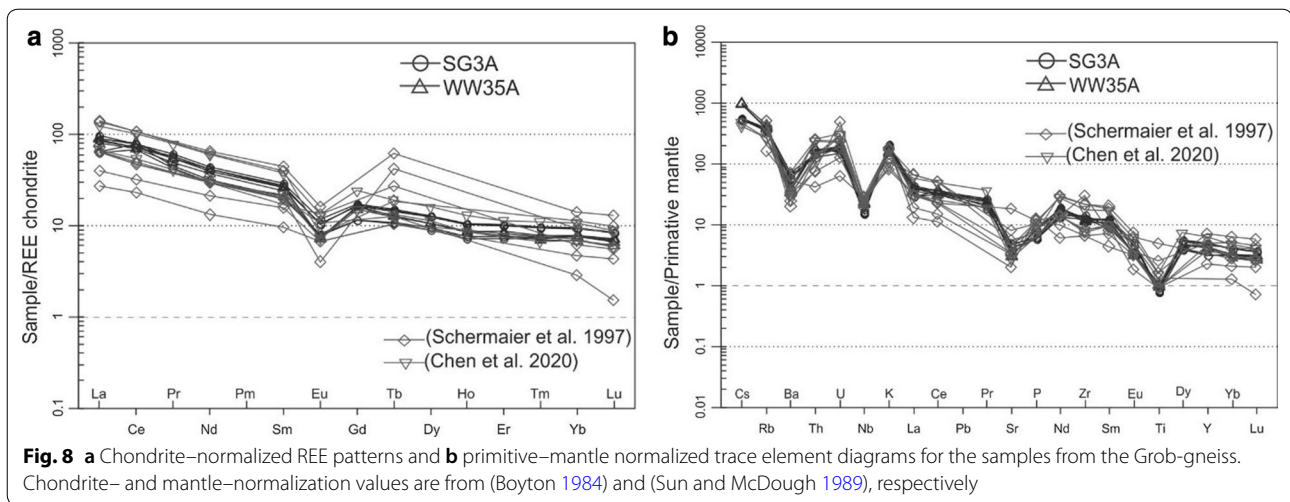
$$A/NK = Al_2O_3 / (Na_2O + K_2O) \text{ (mol \%)}; A/CNK = Al_2O_3 / (CaO + Na_2O + K_2O) \text{ (mol \%)}$$

$$T_{Zr} \text{ (Zircon saturation temperatures, in } ^\circ\text{C)} = 12900 / [2.95 + 0.85 \times M + \ln(496000 / Zr_{\text{mel}})] - 273, \text{ in here } M = [(Na + K + 2Ca) / (Al \times Si)], \text{ all in cation fraction}$$


from I-type granites (Chappell 1999); (3) the presence of inherited zircon grains and the Al-rich minerals muscovite and garnet (Figs. 3, 4; Table 1) are typical for S-type granites (Clemens 2003; Healy et al. 2004); (4) in accordance with the method proposed by Watson and Harrison (1983), the granites from the samples yield zircon saturation temperatures with a range of 769 to 798 °C with an average of 780 °C (Table 3a). Low zircon saturation temperatures are interpreted to represent the maximum temperature of the granitic protolith magma, which are

consistent with those of S-type granites (Chappell and White 1974; Miller et al. 2003).

Furthermore, the studied zircon grains from the samples show $\epsilon_{Hf}(t)$ values of -4.37 to -0.6 , with T_{DM2} values of 1.31–1.55 Ga, which suggests that the zircon grains and thus the granitic magma were derived by reworking of older sedimentary or metamorphic/magmatic continental crust. Based on the above petrographic, geochemical and isotopic distinctions, we conclude that the protoliths of the Permian metagranite in



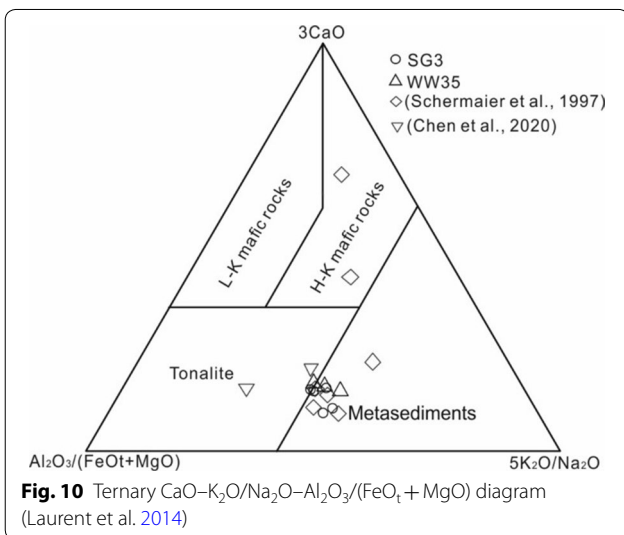
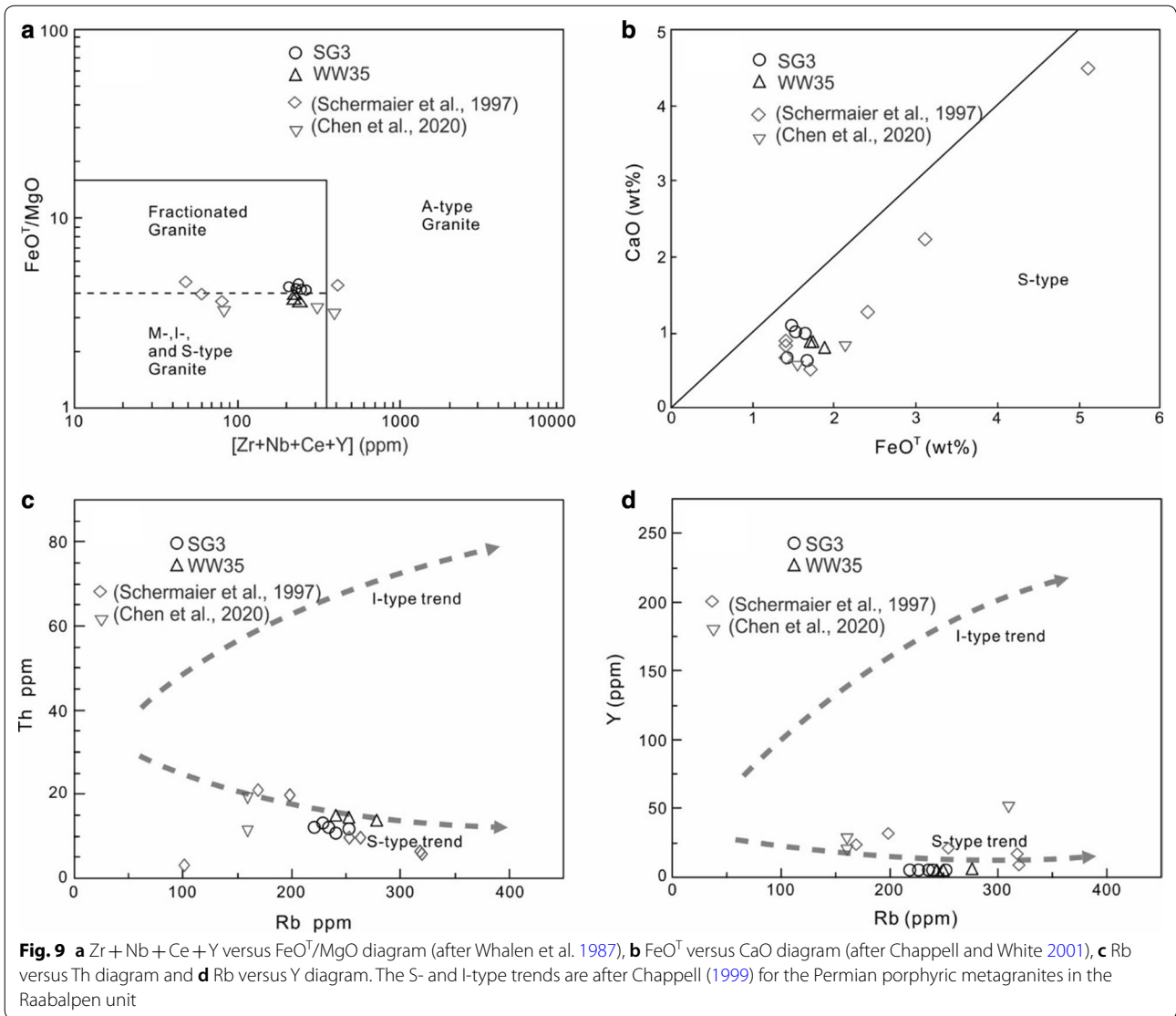
the Raabalpen basement are S-type granites. Additionally, a S-type granite affinity of the metagranites in the Sopron Hills complex was proposed by Chen et al. (2020) and Demény et al. (1997) on the basis of bulk-rock major and trace elements as well as Sr and O isotope geochemistry. Additionally, the porphyric metagranites almost plot in the metasediments field in the ternary $\text{CaO}-\text{K}_2\text{O}/\text{Na}_2\text{O}-\text{Al}_2\text{O}_3/(\text{FeO} + \text{MgO})$ diagram (Laurent et al. 2014) (Fig. 10). In conclusion, the Permian granitic magmatism in the Raabalpen basement area was strictly crust-derived.

6.3 Geodynamic setting and paleogeographic implications

A series of tectonic models has been proposed for Permian geodynamics of the Alps. This contribution presents geochronological constraints (LA-ICP-MS U–Pb dating of zircon) on porphyric metagranites preserved in the Lower Austroalpine unit, Eastern Alps. This is a crucial record for Permian geodynamics.

The Permian evolution in the Alpine realm has already been interpreted as due to underplating of the lower crust by extensive gabbroic intrusions and associated rifting in the Permian (Peressini et al. 2007; Miller et al. 2011; Manzotti et al. 2017; Manzotti et al. 2018; Marotta and Spalla 2007; Petri et al. 2017). However, Schuster et al. (2001b) reviewed the Permian–Triassic thermal event in the Southalpine and Austroalpine units based on many references at that time, and argued that the extensional mechanism attribute to the northward subduction of the Paleotethys, corresponding with the back-arc extension model of Stampfli and Kozur (2006). Alternative view is that the event has been related to the opening of the Neotethys Ocean (Cassinis et al. 2012; Muttoni et al. 2009). But we are agreeing with an intracontinental rift model

with the opening of the Meliata oceanic rift (Neubauer et al. 2000; Putiš et al. 2016; Plašienka 2018), some lines of evidence support this argument. The Permian granite-dominated bimodal magmatism of the Raabalpen Complex argues for a rift setting as well as the Middle Permian timing of magmatism coeval with volcanism associated with post-Variscan clastic sediments, e.g. the acidic Roßkogel volcanics overlying the northern margin of the Raabalpen Complex (Fig. 2). In the extra-Alpine Variscan massifs (Massif Central, Schwarzwald, Bohemian Massif), Permian granites are very rare (Finger et al. 2003) whereas granites of this age are almost ubiquitous in the Alps, such as the Western Alps (e.g. Decarlis et al. 2013; Ballèvre et al. 2018), Southern Alps (e.g. Schaltegger and Brack 2007) and the Eastern Alps (e.g. Schuster et al. 2001a, b; Knoll et al. 2018). Permian granitoids can be traced to the Western Carpathians (Finger et al. 2003; Broska and Kubiš 2018). This comparison is aided by the detailed tectonic and geochronological constraints available for the Western Carpathians. In recent years, many scholars conduct the age, geochemistry and origin of the Permian granitoids (e.g. Broska and Kubiš 2018; Finger and Broska 1999; Kohút and Stein 2005; Radvanec et al. 2009 and references therein) and extrusive equivalents (e.g., Pelech et al. 2017; Putiš et al. 2016; Spišiak et al. 2018; Vozarova et al. 2016 and references therein) preserved in the West Carpathian (Uher et al. 2002). Also, Permian felsic volcanic rocks in the Tisza Mega-unit also interpreted be formed in the extensional setting succeeding the post-collisional environment (Ondrejka et al. 2018; Szemerédi et al. 2020). Moreover, there seems to be a considerable time gap between the Variscan and the Permian granites (Finger et al. 2003), the magmatism should be considered post-orogenic since the orogenic activity in the Variscan belt terminated at the end of the



Westphalian (Dal Piaz 1993; Ziegler 1993) and uppermost Carboniferous intramontane molasse is widespread in the Austroalpine and eastern part of the Southalpine domains (Krainer 1993). The most striking argument is that post-Variscan sedimentary successions start with an angular unconformity and e.g. the Middle Permian Bozen porphyry of the Southalpine units are part of the post-Variscan cover successions started within Late Carboniferous (Hubmann et al. 2014; Krainer 1993). Therefore, these Permian granites in the eastern Austroalpine unit obviously indicate a new tectonomagmatic cycle in the Alpine pre-Mesozoic basement, and are not related to the collapse of the Variscan orogen. In some extra-Alpine Variscan basement areas Permian magmatism and low-pressure metamorphism also occurred, there explained as post-Variscan collapse (Villaros et al. 2018).

As a whole, Permomesozoic syn-rift sequences are spread in overall the Eastern Alps (Neubauer et al. 2018). E.g., the Wechsel window below the Raabalpen basement was filled by a contemporaneous halfgraben volcanic-sedimentary basin (Faupl 1970) (Fig. 11). On the basis of the development of Permian sedimentary units with similar successions of the Carnic Alps and South Karawanken of the eastern Southalpine unit, Neubauer (2016) argued that rifting started already during the Early Permian, and a major extensional event occurred during the Early Permian separating Lower and Upper Permian carbonate platforms (Schaffhauser et al. 2015). In Austroalpine units, rifting occurred later, and the response of lower crust to rifting also includes mafic and acidic magmatism, high-temperature/low-pressure metamorphism (Neubauer 2016; Schuster et al. 2001b; Thöni 1999). In the upper crust, the poorly dated rift-onset unconformity formed in Early or Middle Permian and resulted in N-S to NE-SW striking halfgrabens filled with up to 1.5 km thick terrestrial clastics (Neubauer 2016; Neubauer et al. 2018). Permian to Triassic ductile shear zones with $^{40}\text{Ar}/^{39}\text{Ar}$ sericite ages of 239 and 267 Ma are potentially correlated with these signatures of extensional tectonics (Liu et al. 2001; Neubauer 2016). Age, type and distribution of lower crustal magmatism allows correlation with upper crustal rift basin infill and therefore correlation of detached pieces within the Austroalpine thrust wedge.

Finally, it should be noted that the porphyric metagranites occur only in the Lower Raabalpen basement complex and its equivalent Stuhleck-Kirchberg nappes. However, the overlying Middle and Upper Austroalpine

nappes does virtually not contain Permian (meta)granites except such in southernmost Pohorje Mts. (Chang et al. this issue) hinting towards asymmetric rifting, also the Lower Austroalpine unit did not juxtapose Middle and Upper Austroalpine Unit in that time (Fig. 12). Haas et al. (2020) argued for Jurassic strike-slip to explain juxtaposition of far travelled units in the course of closure of the Meliata ocean and coeval opening of the Penninic Ocean.

7 Conclusions

On the basis of our new LA-ICP-MS zircon U-Pb ages and Hf isotopic compositions, as well as whole-rock geochemical data on metagranitoid rocks in the Raabalpen basement, the following conclusions can be derived:

(1) LA-ICP-MS zircon U-Pb data reveal that the “Grobgneis”-type porphyric metagranite in the Raabalpen basement, Lower Austroalpine Unit, was emplaced at about ~266–~272 Ma, overprinted by the Triassic tectono-thermal events.

(2) The “Grobgneis”-type porphyric metagranites are strongly peraluminous (i.e., typical S-type granites) characterized by high A/CNK values (≥ 1.11), high normative corundum (1.24–1.90%), moderately negative Eu anomalies ($\text{Eu}/\text{Eu}^* = 0.28\text{--}0.81$), and strong negative Ba, Nb, Sr, P and Ti anomalies.

(3) Petrography and whole-rock geochemical data coupled with Hf isotopic compositions ($\varepsilon\text{Hf}(t) = -4.37$ to -0.6) indicate that the protolith derived from recycled continental crustal materials.

(4) We propose rift-related magmatism during the Permian in the Lower Austroalpine unit rather than a

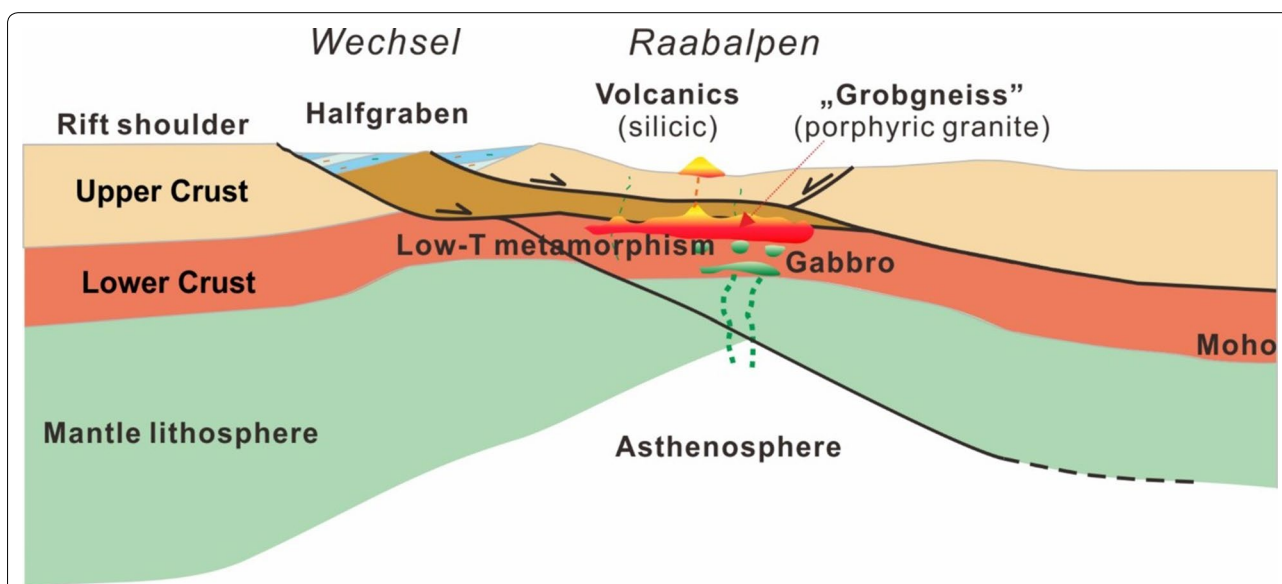
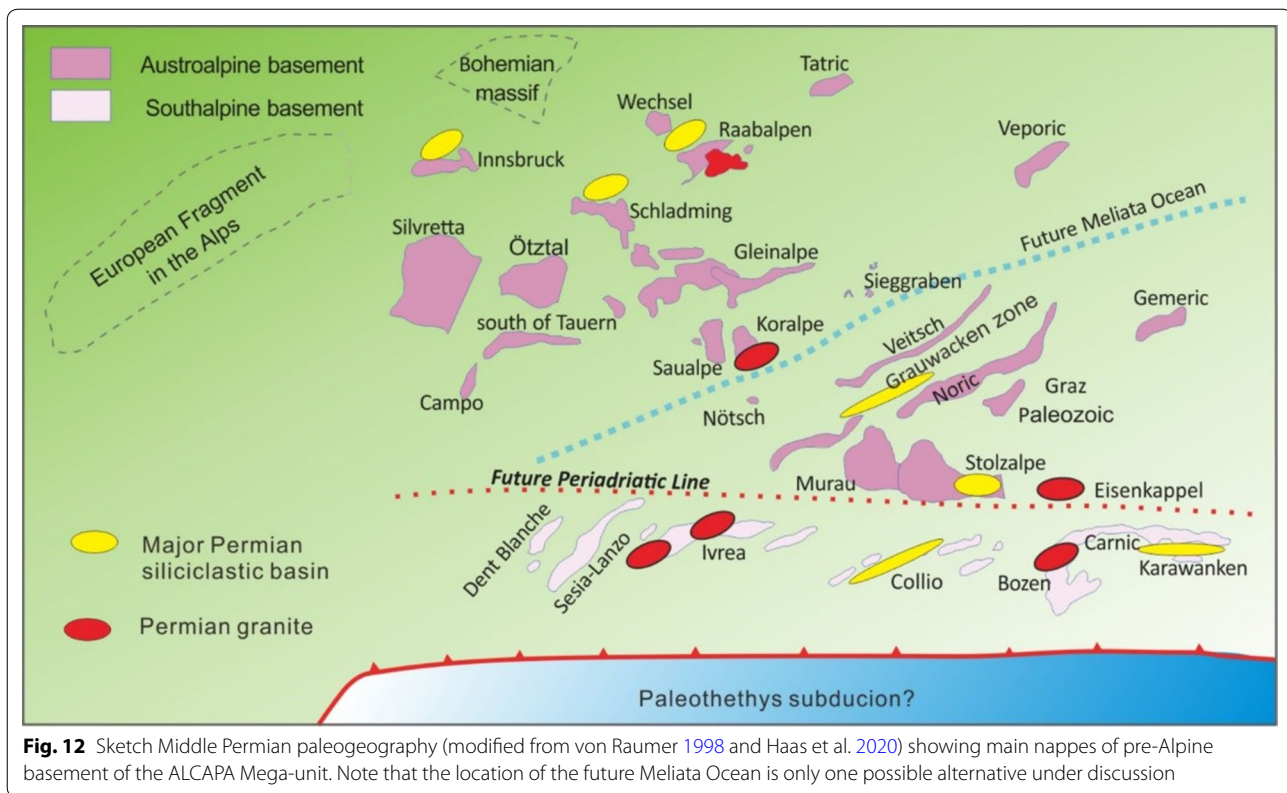


Fig. 11 Schematic diagram showing the tectonic setting of the Permian event in the Raabalpen-Wechsel areas



subduction-related tectonic setting. The continental rifting phase giving rise to this magmatism marks the embryo of the new orogenic cycle. The Permian magmatism coeval with the regional Permian metamorphism is interpreted as resulting from rifting, heralding the opening of the Meliata Ocean in the Eastern Alps and West Carpathians.

Acknowledgements

We acknowledge constructive reviews and comments by two anonymous reviewers and by the guest editor, Paola Manzotti. These helped to clarify ideas and presentation.

Authors' contributions

SY, FN and Y-JL designed the study and collected the samples together with JG, RC, S-YY and BL. Analytical work was mostly done by S-YY, Q-BG and SY. All authors contributed to the interpretation of data and writing of the paper under the lead of SY. All authors read and approved the final manuscript.

Funding

SY received no funding. We acknowledge funding of the analytical work from the NFSC (No. 91755212; No. 41772200), Special Fund of Fundamental Scientific Research Business Expense for Higher School of Central Government (No. ZY20110202), together with the Qingdao Leading innovation talents (19-3-2-19-zhc) to Y.-J. Liu.

Availability of data and materials

The entire new data set is included in the paper.

Ethics approval and consent to participate

Not applicable.

Consent for publication

Not applicable.

Competing interests

The authors declare that they have no competing interests.

Author details

¹ College of Earth Sciences, Institute of Disaster Prevention, Sanhe 065201, Hebei, People's Republic of China. ² Department of Geology and Geography, Paris-Lodron-University of Salzburg, 5020 Salzburg, Austria. ³ Key Lab of Submarine Geoscience and Prospecting Techniques, MOE, Institute for Advanced Ocean Study, College of Marine Geosciences, Ocean University of China, Qingdao 266100, China. ⁴ Ocean University of China, Qingdao 266100, China.

Received: 23 April 2020 Accepted: 10 October 2020

Published online: 11 November 2020

References

- Ballèvre, M., Manzotti, P., & Dal Piaz, G. V. (2018). Pre-Alpine (Variscan) inheritance: A key for the location of the future Valaisian Basin (Western Alps). *Tectonics*, 37, 786–817. <https://doi.org/10.1002/2017TC004633>.
- Bernhard, F., Schitter, F., & Finger, F. (1998). Zur Altersstellung der Lazulith-Quarz-Gänge im unterostalpinen Grogneiskomplex der Nordoststeiermark und des südlichen Niederösterreich. *Mitteilungen des Naturwissenschaftlichen Vereines für Steiermark*, 128, 43–56.
- Bonin, B. (2007). A-type granites and related rocks: Evolution of a concept, problems and prospects. *Lithos*, 97, 1–29.
- Bouvier, A., Verwoort, J. D., & Patchett, P. J. (2008). The Lu–Hf and Sm–Nd isotopic composition of CHUR: Constraints from unequilibrated chondrites and implications for the bulk composition of terrestrial planets. *Earth and Planetary Science Letters*, 273, 48–57.

- Boyton, W. R. (1984). Cosmochemistry of the rare earth elements meteorite studies. In P. Henderson (Ed.), *Rare Earth Element Geochemistry* (pp. 63–114). Amsterdam: Elsevier.
- Broska, I., & Kubiš, M. (2018). Accessory minerals and evolution of tin-bearing S-type granites in the western segment of the Gemic Unit (Western Carpathians). *Geologica Carpathica*, 69, 483–497.
- Cassinis, G., Perotti, C. R., & Ronchi, A. (2012). Permian continental basins in the Southern Alps (Italy) and peri-Mediterranean correlations. *International Journal of Earth Sciences*, 101, 129–157.
- Chappell, B. W. (1999). Aluminium saturation in I- and S-type granites and the characterization of fractionated haplogranites. *Lithos*, 46, 535–551.
- Chappell, B. W., & White, A. J. R. (1974). Two contrasting granite types. *Pacific Geology*, 7, 173–174.
- Chappell, B. W., & White, A. J. R. (2001). Two contrasting granite types: 25 years later. *Australian Journal of Earth Sciences*, 48, 489–499.
- Chen, Y.-X., Demény, A., Schertl, H.-P., Zheng, Y.-F., Huang, F., Zhou, K., Jin, Q.-Z., & Xia, X.-P. (2020). Tracing subduction zone fluids with distinct Mg isotope compositions: Insights from high-pressure metasomatic rocks (leucophyllites) from the Eastern Alps. *Geochimica et Cosmochimica Acta*, 271, 154–178.
- Clemens, J. D. (2003). S-type granitic magmas—petrogenetic issues, models and evidence. *Earth-Science Reviews*, 61, 1–18.
- Dal Piaz, G. V. (1993). Evolution of Austro-alpine and Upper Penninic basement in the North Western Alps from Variscan convergence to post-Variscan extension. In J. E. von Raumer & E. Neubauer (Eds.), *Pre-Mesozoic Geology in the Alps* (pp. 327–344). Berlin: Springer-Verlag.
- Dallmeyer, R. D., Handler, R., Neubauer, F., & Fritz, H. (1998). Sequence of thrusting within a thick-skinned tectonic wedge: Evidence from $^{40}\text{Ar}/^{39}\text{Ar}$ ages from the Austroalpine nappe complex of the Eastern Alps. *Journal of Geology*, 106, 71–86.
- Decarlis, A., Dallagiovanna, G., Lualdi, A., Maino, M., & Seno, S. (2013). Strati-graphic evolution in the Ligurian Alps between Variscan heritages and the Alpine Tethys opening: A review. *Earth-Science Reviews*, 125, 43–68.
- Demény, A., Sharp, Z. D., & Pfeifer, H.-R. (1997). Mg-metasomatism and formation conditions of Mg-chlorite-muscovite-quartzphyllites (leucophyllites) of the Eastern Alps (W. Hungary) and their relations to Alpine whiteschists. *Contributions to Mineralogy and Petrology*, 128, 247–260.
- Deroin, J.-P., & Bonin, B. (2003). Late Variscan tectonomagmatic activity in Western Europe and surrounding areas: The mid-Permian Episode. *Bollettino della Società Geologica Italiana*, 2, 169–184.
- Doblas, M., Oyarzun, R., López-Ruiz, J., Cebriá, J. M., Youbi, N., Mahecha, V., Lago, M., Pocoví, A., & Cabanis, B. (1998). Permo-Carboniferous volcanism in Europe and northwest Africa: a superplume exhaust valve in the centre of Pangaea? *Journal of African Earth Sciences*, 26, 89–99.
- Faupl, P. (1970). Zur Geologie des NW-Abschnitts des Wechselgebietes zwischen Trattenbach (NÖ) und Frörschnitz (Stmk.) — Österreich. *Mitteilungen der Gesellschaft der Geologie und Bergbaustudenten Wien*, 19, 27–70.
- Finger, F., & Broska, I. (1999). The Gemic S-type granites in southeastern Slovakia: Late Palaeozoic or Alpine intrusions? Evidence from electron-microprobe dating of monazite. *Schweizerische Mineralogische und Petrographische Mitteilungen*, 79, 439–443.
- Finger, F., Broska, I., Haunschmid, B., Hrasko, L., Kohút, M., Krenn, E., et al. (2003). Electron-microprobe dating of monazites from Western Carpathian basement granitoids: plutonic evidence for an important Permian rifting event subsequent to Variscan crustal anatexis. *International Journal of Earth Sciences*, 92, 86–98.
- Finger, F., & Steyrer, H. P. (1990). I-type granitoids as indicators of a late Paleozoic convergent ocean-continent margin along the southern flank of the central European Variscan orogen. *Geology*, 18, 1207–1210.
- Flügel, H.W., & Neubauer, F. (1984). Steiermark. Erläuterungen zur Geologischen Karte der Steiermark 1:200,000. *Geol. Bundesanstalt, Wien*, 1–127.
- Frost, B. R., Barnes, C. G., Collins, W. J., Arculus, R. J., Ellis, D. J., & Frost, C. D. (2001). A geochemical classification for granitic rocks. *Journal of Petrology*, 42, 2033–2048.
- Griffin, W. L., Wang, X., Jackson, S. E., Pearson, N. J., O'Reilly, S. Y., Xu, X., et al. (2002). Zircon chemistry and magma mixing, SE China: In-situ analysis of Hf isotopes, Tonglu and Pingtan igneous complexes. *Lithos*, 61, 237–269.
- Haas, I., Eichinger, S., Haller, D., Fritz, H., Nievoll, J., Mandl, M., et al. (2020). Gondwana fragments in the Eastern Alps: A travel story from U/Pb zircon data. *Gondwana Research*, 77, 204–222.
- Healy, B., Collins, W. J., & Richards, S. W. (2004). A hybrid origin for Lachlan S-type granites: the Murrumbidgee Batholith example. *Lithos*, 78, 197–216.
- Hoinkes, G., Koller, F., & Rantitsch, G. (1999). Alpine metamorphism of the Eastern Alps. *Schweizerische Mineralogische und Petrographische Mitteilungen*, 79, 155–181.
- Hoskin, P. W. O., & Schaltegger, U. (2003). The composition of zircon and igneous and metamorphic petrogenesis. *Reviews of Mineralogy and Geochemistry*, 53, 27–62.
- Hou, K. J., Li, Y. H., & Tian, Y. Y. (2009). In situ U-Pb zircon dating using laser ablation-multi ion counting-ICP-MS. *Mineral Deposits*, 28, 481–492. **(in Chinese with English abstract)**.
- Hou, K. J., Yanhe, L. I., & Xie, G. Q. (2007). Laser ablation-MC-ICP-MS technique for Hf isotope microanalysis of zircon and its geological applications. *Acta Petrologica Sinica*, 23, 2595–2604.
- Hubmann B., Ebner F., Ferretti A., Kido E., Krainer K., Neubauer F., Schönlaub H.P., & Suttner, T.J., 2014. The Paleozoic Era(theme). *Abhandlungen der Geologischen Bundesanstalt*, 66 (Sec. Ed.), 9–135.
- Jackson, S. E., Pearson, N. J., Griffin, W. L., & Belousova, E. A. (2004). The application of laser ablation-inductively coupled plasma-mass spectrometry (LA-ICP-MS) to in situ U-Pb zircon geochronology. *Chemical Geology*, 211, 47–69.
- Jochum, K. P., Nohl, U., Herwig, K., Lammel, E., Stoll, B., & Hofmann, A. W. (2005). GeoReM: A new geochemical database for reference materials and isotopic standards. *Geostandards and Geoanalytical Research*, 29, 333–338.
- Klötzli, U. S., Sinigoi, S., Quick, J. E., Demarchi, G., Tassinari, C. C. G., Sato, K., et al. (2014). Duration of igneous activity in the Sesia Magmatic System and implications for high-temperature metamorphism in the Ivrea-Verbano deep crust. *Lithos*, 206–207, 19–33.
- Knoll, T., Schuster, R., Huet, B., Mali, H., Onuk, P., Horschneig, M., et al. (2018). Spodumene Pegmatites and related leucogranites from the Austro-Alpine Unit (Eastern Alps, Central Europe): Field relations, petrography, geochemistry, and geochronology. *The Canadian Mineralogist*, 56, 489–528.
- Kohút, M., & Stein, H. (2005). Re–Os molybdenite dating of granite-related Sn–W–Mo mineralisation at Hnilec, Gemic Superunit, Slovakia. *Mineralogy and Petrology*, 85, 117–129.
- Kozur, H. (1991). The Evolution of the Meliata-Hallstatt ocean and its significance for the early evolution of the Eastern Alps and Western Carpathians. *Palaeogeography, Palaeoclimatology, Palaeoecology*, 87, 109–135.
- Krainer, K. (1993). Late- and post-Variscan sediments of the Eastern and Southern Alps. In J. von Raumer & F. Neubauer (Eds.), *Pre-Mesozoic Geology in the Alps* (pp. 537–564). Berlin: Springer.
- Kunz, B., Manzotti, P., von Niederhäusern, B., Engi, M., Giuntoli, F., & Lanari, P. (2018). Permian high temperature metamorphism in the Western Alps (NW Italy). *International Journal of Earth Sciences*, 107, 203–229.
- Laurent, O., Martin, H., Moyon, J. F., & Doucelance, R. (2014). The diversity and evolution of late-Archean granitoids: Evidence for the onset of “modern-style” plate tectonics between 3.0 and 2.5Ga. *Lithos*, 205, 208–235.
- Liu, Y., Gao, S., Hu, Z., Gao, C., Zong, K., & Wang, D. (2010). Continental and Oceanic Crust Recycling-induced Melt-Peridotite Interactions in the Trans-North China Orogen: U-Pb Dating, Hf Isotopes and Trace Elements in Zircons from Mantle Xenoliths. *Journal of Petrology*, 51, 537–571.
- Liu, Y., Genser, J., Handler, R., Friedl, G., & Neubauer, F. (2001). $^{40}\text{Ar}/^{39}\text{Ar}$ muscovite ages from the Penninic/Austroalpine plate boundary, Eastern Alps. *Tectonics*, 20, 528–547.
- Liu, Y., Hu, Z. C., Gao, S., Günther, D., Xu, J., Gao, C. G., et al. (2008). In situ analysis of major and trace elements of anhydrous minerals by LA-ICP-MS without applying an internal standard. *Chemical Geology*, 257, 34–43.
- Liu, Y., Liu, X. M., Hu, Z. C., Diwu, C. R., Yuan, H. L., & Gao, S. (2007). Evaluation of accuracy and long-term stability of determination of 37 trace elements in geological samples by ICP-MS. *Acta Petrologica Sinica*, 23, 1203–1210. **(in Chinese with English abstract)**.
- Lizuka, T., & Hirata, T. (2005). Improvements of precision and accuracy in situ Hf isotope microanalysis of zircon using the laser ablation-MC-ICPMS technique. *Chemical Geology*, 220, 121–137.
- Ludwig, K. R. (2003). *Isoplot 3.00: A Geochronological Toolkit for Microsoft Excel*. Berkeley: Berkeley Geochronology Center.
- Mandl, M., Kurz, W., Hauzenberger, C., Fritz, H., Klötzli, U., & Schuster, R. (2018). Pre-Alpine evolution of the Seckau Complex (Austroalpine basement/Eastern Alps): Constraints from in situ LA-ICP-MS U-Pb zircon

- geochronology. *Lithos*, 296–299, 412–430. <https://doi.org/10.1016/j.lithos.2017.11.022>.
- Maniar, P. D., & Piccoli, P. M. (1989). Tectonic discrimination of granitoids. *GSA GSA Bulletin*, 101, 635–643.
- Manzotti, P., Ballèvre, M., & Dal Piaz, G. V. (2017). Continental gabbros in the Dent Blanche Tectonic System (Western Alps): From the pre-Alpine crustal structure of the Adriatic palaeo-margin to the geometry of an alleged subduction interface. *Journal of the Geological Society London*, 174, 541–556.
- Manzotti, P., Rubatto, D., Zucali, M., El Korh, A., Cenki-Tok, B., Ballèvre, M., et al. (2018). Permian magmatism and metamorphism in the Dent Blanche nappe: Constraints from field observations and geochronology. *Swiss Journal of Geosciences*, 111, 79–97.
- Marotta, A.M. & Spalla, M.I. (2007). Permian-Triassic high thermal regime in the Alps: Result of late Variscan collapse or continental rifting? Validation by numerical modeling. *Tectonics*, 26, TC4016, <https://doi.org/10.1029/2006TC002047>.
- Ménard, G., & Molnar, P. (1988). Collapse of a Hercynian Tibetan plateau into Late Palaeozoic European basin and range province. *Nature*, 334, 235–237.
- Middlemost, E. A. K. (1994). Naming materials in the magma/igneous rock system. *Earth-Science Reviews*, 37, 215–224.
- Miller, C. F. (1985). Are Strongly Peraluminous Magmas Derived from Pelitic Sedimentary Sources? *The Journal of Geology*, 93, 673–689.
- Miller, C. F., McDowell, S. M., & Mapes, R. W. (2003). Hot and cold granites? Implications of zircon saturation temperatures and preservation of inheritance. *Geology*, 31, 529–532.
- Miller, C., Thöni, M., Goessler, W., & Tessadori, R. (2011). Origin and age of the Eisenkappel gabbro to granite suite (Carinthia, SE Austrian Alps). *Lithos*, 125, 434–448.
- Miller, C., Thöni, M., Konzett, J., Kurz, W., & Schuster, R. (2005). Eclogites from the Koralpe and Saualpe type-localities, eastern Alps, Austria. *Mitteilungen der Österreichischen Mineralogischen Gesellschaft*, 150, 227–263.
- Morauf, W. (1980). Die permische Differentiation und die alpidische Metamorphose des Granitgneises von Wolfsberg (Koralpe) mit Rb-Sr- und K-Ar-Isotopenbestimmung. *Tschermak's Mineralogische und Petrographische Mitteilungen*, 27, 169–185.
- Morel, M. L. A., Nebel, O., Nebel-Jacobsen, Y. J., Miller, J. S., & Vroon, P. Z. (2008). Hafnium isotope characterization of the GJ-1 zircon reference material by solution and laser-ablation MC-ICPMS. *Chemical Geology*, 255, 231–235.
- Müller, W., Dallmeyer, R. D., Neubauer, F., & Thöni, M. (1999). Deformation-induced resetting of Rb/Sr and ⁴⁰Ar/³⁹Ar mineral systems in a low-grade, polymetamorphic terrane (Eastern Alps, Austria). *Journal of the Geological Society (London)*, 156, 261–278.
- Muttoni, G., Gaetani, M., Kent, D. V., Sciunnach, D., Angiolini, L., Berra, F., et al. (2009). Opening of the Neo-Tethys Ocean and the Pangea B to Pangea A transformation during the Permian. *GeoArabia*, 14, 17–46.
- Neubauer, F. (1988). The Variscan orogeny in the Austroalpine and Southalpine domains of the Eastern Alps. *Schweizerische Mineralogische und Petrographische Mitteilungen*, 68, 339–349.
- Neubauer, F. (2016). Permian and Triassic Meliata-related rift and drift processes in Eastern Alps: Middle and lower crust and its potential correlation with sedimentary units. *Geophysical Research Abstracts*, 18, EGU2016-4604.
- Neubauer, F. & Frisch, W. (1993). The Austroalpine metamorphic basement east of the Tauern window. In J. von Raumer & F. Neubauer (Eds.) *Pre-Mesozoic Geology in the Alps* (pp. 515–536). Heidelberg: Springer.
- Neubauer, F., Genser, J., & Handler, R. (2000). The Eastern Alps: Result of a two-stage collision process. *Mitt. Oesterr. Geol. Ges.*, 92, 117–134.
- Neubauer, F., Genser, J., Heberer, B., Etzel, A., & Stauber, O. (2018). Field Trip Post-EX-1 Transect across the Eastern Alps. XXI International Congress of the CBGA, Salzburg, Austria, September 10–13, 2018, Berichte der Geologischen Bundesanstalt, 126, p. 137–222.
- Neubauer, F., Hoinkes, G., Sassi, F. P., Handler, R., Höck, V., Koller, F., & Frank, W. (1999). Pre-Alpine metamorphism of the Eastern Alps. *Schweizerische Mineralogische und Petrographische Mitteilungen*, 79, 41–62.
- Neubauer, F., Müller, W., Peindl, P., Mozschevitz, E., Wallbrecher, E., & Thöni, M. (1992). Evolution of lower Austroalpine units along the eastern margins of the Alps: A review. In F. Neubauer (Ed.), *ALCAPA Field Guide* (pp. 97–114). Graz: University of Graz.
- Nievol, J. (1984). Der Südrand der Grauwackenzone zwischen Stübmring und Neuberg (Obersteiermark, OK 103 Kindberg). *Mitteilungen der Österreichischen Geologischen Gesellschaft*, 77, 63–71.
- Ondrejka, M., Li, X.-H., Vojtko, R., Putiš, M., Uher, P., & Sobocký, T. (2018). Permian A-type rhyolites of the Muráň Nappe, Inner Western Carpathians, Slovakia: In situ zircon U-Pb SIMS ages and tectonic setting. *Geologica Carpathica*, 69, 187–198.
- Passchier, C. W., & Trouw, R. A. J. (1998). *Microtectonics (second edition)* (p. 289). Berlin Heidelberg: Springer-Verlag.
- Pelech, O., Vožarova, A., Uher, P., Petřík, I., Plašienka, D., Šarinová, K., et al. (2017). Late Permian volcanic dykes in the crystalline basement of the Považský Inovec Mts. (Western Carpathians): U-Th-Pb zircon SHRIMP and monazite chemical dating. *Geologica Carpathica*, 68, 530–542.
- Pereira, M. F., Castro, A., Chichorro, M., Fernández, C., Díaz-Alvarado, J., Martí, J., et al. (2014). Chronological link between deep-seated processes in magma chambers and eruptions: Permo-Carboniferous magmatism in the core of Pangaea (Southern Pyrenees). *Gondwana Research*, 25, 290–308.
- Peressini, G., Quick, J. E., Sinigoi, S., Hofmann, A. W., & Fanning, M. (2007). Duration of a large mafic intrusion and heat transfer in the lower crust: A SHRIMP U-Pb Zircon Study in the Ivrea-Verbano Zone (Western Alps, Italy). *Journal of Petrology*, 48, 1185–1218.
- Petri, B., Mohn, G., Skrzypek, E., Mateeva, T., Galster, F., & Manatschal, G. (2017). U-Pb geochronology of the Sondalo gabbroic complex (Central Alps) and its position within the Permian post-Variscan extension. *International Journal of Earth Sciences*, 106, 2873–2893.
- Plašienka, D. (2018). Continuity and episodicity in the early Alpine tectonic evolution of the Western Carpathians: How large-scale processes are expressed by the orogenic architecture and rock record data. *Tectonics*, 37, <https://doi.org/10.1029/2017TC004779>.
- Putiš, M., Korikovsky, S. P., Wallbrecher, E., Unzog, W., Olesen, N., & Fritz, H. (2002). Evolution of an eclogitized continental fragment in the Eastern Alps (Sieggraben, Austria). *Journal of Structural Geology*, 24, 339–357.
- Putiš, M., Li, J., Ružička, P., Ling, X., & Nemeč, O. (2016). U/Pb SIMS zircon dating of a rhyolite intercalation in Permian siliciclastics as well as a rhyodacite dyke in micaschists (Infrataticum, W. Carpathians). *Mineralia Slovaca*, 48, 99–108.
- Putiš, M., Soták, J., Li, Q. L., Ondrejka, M., Li, X.-H., Hu, Z.-C., et al. (2019). Origin and Age Determination of the Neotethys Meliata Basin Ophiolite Fragments in the Late Jurassic-Early Cretaceous Accretionary Wedge Mélange (Inner Western Carpathians, Slovakia). *Minerals*, 9, 652. <https://doi.org/10.3390/min9110652>.
- Radvanec, M., Konečný, P., Ondrejka, M., Putiš, M., Uher, P., & Nemeth, Z. (2009). The Gemic granites as an indicator of the crustal extension above the Late-Variscan subduction zone and during the Early Alpine riftogenesis (Western Carpathians): An interpretation from the monazite and zircon ages dated by CHIME and SHRIMP methods. *Miner Slov*, 41, 381–394.
- Rickwood, P. C. (1989). Boundary lines within petrologic diagrams which use oxides of major and minor elements. *Lithos*, 22, 247–263.
- Rodríguez-Méndez, L., Cuevas, J., & Tubía, J. M. (2016). Post-Variscan basin evolution in the central Pyrenees: Insights from the Stephanian-Permian Anayet Basin. *Comptes Rendus Geoscience*, 348, 333–341.
- Rubatto, D. (2017). Zircon: The Metamorphic Mineral. *Reviews in Mineralogy and Geochemistry*, 83, 261–295.
- Schaffhauser, M., Krainer, K., & Sanders, D. (2015). Early Permian carbonate shelf margin deposits: The type section of the Trogkofel Formation (Artinskian/Kungurian), Carnic Alps, Austria/Italy. *Austrian Journal of Earth Sciences*, 108(2), 277–301.
- Schaltegger, U., & Brack, P. (2007). Crustal-scale magmatic systems during intracontinental strike-slip tectonics: U, Pb and Hf isotopic constraints from Permian magmatic rocks of the Southern Alps. *International Journal of Earth Sciences*, 96, 1131–1151.
- Schermaier, A., Haunschmid, B., & Finger, F. (1997). Distribution of Variscan I- and S-type granites in the Eastern Alps: A possible clue to unravel pre-Alpine basement structures. *Tectonophysics*, 272, 315–333.
- Schmid, S. M., Fügenschuh, B., Kissling, E., & Schuster, R. (2004). Tectonic map and overall architecture of the Alpine orogen. *Eclogae Geologicae Helvetiae*, 97, 93–117.
- Schuster, K., Berka, R., Draganits, E., Frank, W., & Schuster, R. (2001a). Lithologie, Metamorphosegeschichte und tektonischer Bau der kristallinen

- Einheiten am Alpenostrand. *Geologische Bundesanstalt Arbeitstagung 2001 – Neuberg an der Mürz, Beiträge*, 29–56, Wien.
- Schuster, R., Scharbert, S., Abart, R., & Frank, W. (2001b). Permo-Triassic extension and related HT/LP metamorphism in the Austroalpine - Southalpine realm. *Mitt. Ges. Geol. Bergbaustud. Österr.*, 45, 111–141.
- Schuster, R., & Stüwe, K. (2008). Permian metamorphic event in the Alps. *Geology*, 36, 603–606.
- Söderlund, U., Patchett, P. J., Vervoort, J. D., & Isachsen, C. E. (2004). The 176Lu decay constant determined by Lu–Hf and U–Pb isotope systematics of Precambrian mafic intrusions. *Earth and Planetary Science Letters*, 219, 311–324.
- Spišiak, J., Vetráková, L., Chew, D., Ferenc, Š., Mikuš, T., Šimonová, V., et al. (2018). Petrology and dating of the Permian lamprophyres from the Malá Fatra Mts. (Western Carpathians, Slovakia). *Geologica Carpathica*, 69, 453–466.
- Stampfli, G. M., & Kozur, H. W. (2006). Europe from the Variscan to the Alpine cycle. *Geological Society, London, Memoirs*, 32, 57–82.
- Sun, S. S., & McDough, W. F. (1989). Chemical and isotope systematics of oceanic basalts: Implications for mantle composition and processes. In A. D. Saunders (Ed.), *Magmatism in ocean Basins* (pp. 313–345). London: Geological Society of London Special Publication.
- Szemerédi, M., Lukács, R., Varga, A., Dunkl, I., Józsa, S., Tatu, M., et al. (2020). Permian felsic volcanic rocks in the Pannonian Basin (Hungary): New petrographic, geochemical, and geochronological results. *International Journal of Earth Sciences*, 109, 101–125.
- Thöni, M. (1999). A review of geochronological data from the Eastern Alps. *Schweizerische Mineralogische und Petrographische Mitteilungen*, 79, 209–230.
- Thöni, M., & Jagoutz, E. (1992). Some new aspects of dating eclogites in orogenic belts: Sm–Nd, Rb–Sr, and Pb–Pb isotopic results from the Austroalpine Saulape and Koralpe type-locality (Carinthia/Styria, southeastern Austria). *Geochimica et Cosmochimica Acta*, 56, 347–368.
- Thöni, M., & Miller, C. (1996). Garnet Sm–Nd data from the Saulape and the Koralpe (Eastern Alps, Austria): Chronological and P–T constraints on the thermal and tectonic history. *Journal of Metamorphic Geology*, 14, 453–466.
- Thöni, M., & Miller, C. (2009). The “Permian event” in the Eastern European Alps: Sm–Nd and P–T data recorded by multi-stage garnet from the Plankogel unit. *Chemical Geology*, 260, 20–36.
- Tropper, P., Harlov, D., Krenn, E., Finger, F., Rhede, D., & Bernhard, F. (2007). Zr-bearing minerals as indicators for the polymetamorphic evolution of the eastern, lower Austroalpine nappes (Stubenberg Granite contact aureole, Styria, Eastern Alps, Austria). *Lithos*, 95, 72–86.
- Uher, P., Ondrejka, M., Spišiak, J., Broska, I., & Putiš, M. (2002). Lower Triassic potassium-rich rhyolites of the Silicic Unit, Western Carpathians, Slovakia: Geochemistry, mineralogy and genetic aspects. *Geologica Carpathica*, 53, 27–36.
- Villaras, A., Laurent, O., Couzinié, S., Moyon, J. F., & Mintrone, M. (2018). Plutons and domes: The consequences of anatectic magma extraction—example from the southeastern French Massif Central. *International Journal of Earth Sciences*, 107, 2819–2842.
- Visonà, D., Fioretti, A. M., Poli, M. E., Zanferrari, A., & Fanning, M. (2007). U–Pb SHRIMP zircon dating of andesite from the Dolomite area (NE Italy): Geochronological evidence for the early onset of Permian Volcanism in the eastern part of the southern Alps. *Swiss Journal of Geosciences*, 100, 313–324.
- von Raumer, J. F. (1998). The Palaeozoic evolution in the Alps: From Gondwana to Pangea. *Geologische Rundschau*, 87, 407–435.
- Vozarova, A., Rodionov, N., Vozar, J., Lepekina, E., & Sarinova, K. (2016). U–Pb zircon ages from Permian volcanic rocks and tonalite of the Northern Veporicum (Western Carpathians). *Journal of Geosciences*, 61, 221–237.
- Watson, E. B., & Harrison, T. M. (1983). Zircon saturation revisited: Temperature and composition effects in a variety of crustal magma types. *Earth and Planetary Science Letters*, 64, 295–304.
- Whalen, J. B., Currie, K. L., & Chappell, B. W. (1987). A-type granites: geochemical characteristics, discrimination and petrogenesis. *Contributions to Mineralogy and Petrology*, 95(4), 407–419.
- Xie, L. W., Zhang, Y. B., Zhang, H. H., Sun, J. F., & Wu, F. Y. (2008). In situ simultaneous determination of trace elements, U–Pb and Lu–Hf isotopes in zircon and baddeleyite. *Chinese Science Bulletin*, 53, 1565–1573. **(in Chinese with English abstract)**.
- Ziegler, P. A. (1993). Late Palaeozoic–Early Mesozoic plate reorganization: Evolution and demise of the Variscan fold belt. In J. F. von Raumer & F. Neubauer (Eds.), *The Pre-Mesozoic Geology in the Alps* (pp. 203–216). Heidelberg: Springer.

Publisher's Note

Springer Nature remains neutral with regard to jurisdictional claims in published maps and institutional affiliations.

Submit your manuscript to a SpringerOpen® journal and benefit from:

- Convenient online submission
- Rigorous peer review
- Open access: articles freely available online
- High visibility within the field
- Retaining the copyright to your article

Submit your next manuscript at ► [springeropen.com](https://www.springeropen.com)